Region of Attraction Estimation for DC Microgrids with Constant Power Loads Using Potential Theory

Fangyuan Chang, *Student Member*, *IEEE*; Xiaofan Cui, *Student Member*, *IEEE*
Mengqi Wang, *Senior Member*, *IEEE*; Wencong Su, *Senior Member, IEEE*

***Abstract*—The stability issues of DC power grids are attracting researchers' attention, especially with the increasing adoption of power electronic devices and nonlinear loads. Large-signal stability analysis is required to detect and avoid large disturbance and destabilization, which can cause detrimental effects on DC power grids. However, the issue is still unsolved due to the complicated dynamics of large-scale power grids. This paper develops a novel method for estimation of the region of attraction (ROA) with less conservativeness using the Brayton-Moser mixed potential theory. This reliable and robust ROA estimation method provides useful insights into the stable operation of DC power grids. Moreover, this paper reveals the weak correlation between the state variables[1] of branch currents and system stability. It makes it possible to reduce computational cost and lessen the curse of dimensionality by separating these state variables. The case study shows that the proposed approach can obtain a much less conservative ROA compared to traditional methods such as Lyapunov's method.**

***Index Terms*—power electronics-dominated power grids, large-signal stability, region of attraction (ROA) estimation, potential theory, constant power loads.**

I. Introduction

MODERN DC power grids have seen a renaissance in recent years, equipped with more complicated power electronic devices and nonlinear power loads, such as constant power loads (CPLs). Modern DC grids have several unique advantages compared to AC power systems, for example, increased efficiency of power conversion, less copper, and higher power density. However, the distinct DC-grid characteristics of direct P-V coupling and low system inertia pose great challenges to grid stability. Even a small load or generation change can lead to voltage flickers and equipment malfunctions.

The stability issues of DC power grids are attracting researchers' attention. Stability analysis of DC grids can be categorized into two groups: small-signal analysis and large-signal analysis. Most stability studies of DC microgrids are performed using small-signal and linearized models, especially for large-scale DC microgrids with multiple converters and CPLs. Small-signal stability can ensure the stability of the system in the vicinity of the equilibrium point, but the boundary of the stability region cannot be determined and there are limitations when the system has large disturbances. Additionally, linearized models of microgrids are not always applicable because the power converter dynamics can be approximated by a nonlinear state-space averaging model only if the system bandwidth is well below the switching frequency [1]. In contrast, large-signal stability analysis is required to detect and avoid large disturbance and destabilization, which can cause detrimental effects on DC power grids. Large-signal stability analysis can determine the safe operation regions of power grids going through large disturbances. In control theory, the region of attraction (ROA) of complex dynamic systems is a reliable measure of stability level and system robustness against external disturbances. Reliable ROA estimation provides useful insights into the stable operation of DC power grids from the perspective of controlled dynamic systems. The ROA ensures safe operation in the event of a large disturbance, such as load switching, pulse power load, and faults, which is possible in the real-world operation of DC microgrids.

There have been some recent studies on large-signal stability analysis and ROA estimation. Some of these studies were developed based on the design of Lyapunov-based controllers. Grid stability can be guaranteed during the design procedure of Lyapunov-based controllers. Paper [2] presents the stability analysis for a hybrid DC microgrid using nonlinear backstepping controllers (NBCs). The controller is designed to control the output power as well as to minimize the mismatch between generation and consumption while maintaining stable voltages. The design of the controller for each component of the microgrid is based on the Lyapunov theory. The stability analysis is through the formulation of control Lyapunov functions (CLFs), and the theoretical stability is ensured through the negative semi-definiteness of the derivatives of CLFs. In papers [3] and [4], input-to-state-stability (ISS) Lyapunov-based distributed control is proposed for DC microgrids, which realizes a Lyapunov-based power sharing while stabilizing the grid. The distributed controllers are dedicated to grid voltage regulation to effectively stabilize a DC microgrid. A Lyapunov function composed of different Lyapunov functions is investigated to guarantee stability. Paper [5] proposes a robust nonlinear control approach to solve the instability problem of a buck converter with a CPL in DC microgrids. The approach is developed based on passivity-based control (PBC), which guarantees system stability due to its characteristic of transient energy dissipation. Moreover, there are some other approaches not relying on Lyapunov-based controllers that investigate the stability of microgrids with established architecture. In paper [6], the Takagi–Sugeno (TS) fuzzy model is applied to estimate the ROA for a given electric system, which includes a DC power supply and a constant power load connected

[1] Here, the "state variables" refer to several branch currents, defined as $i = [I_{p1}, I_{p2}, \dots, I_{pN}, I_{q1}, I_{q2}, \dots, I_{qN}, I_{t1}, I_{t2}, \dots, I_{tN}, I_{f1}, \dots, I_{fM}]$ in the manuscript, which show a weak correlation with system stability. $I_{p1}, I_{p2}, \dots, I_{pN}$ are the branch currents through source-side resistors $R_{p1}, R_{p2}, \dots R_{pN}$, respectively. $I_{q1}, I_{q2}, \dots, I_{qN}$ are the branch currents through source-side resistors $R_{q1}, R_{q2}, \dots R_{qN}$, respectively. $I_{t1}, I_{t2}, \dots, I_{tN}$ are the currents through source-side transmission line resistors $R_{t1}, R_{t2}, \dots R_{tN}$, respectively. $I_{f1}, \dots, I_{fM}$ are the currents through load-side transmission line resistors $R_{f1}, R_{f2}, \dots R_{fN}$, respectively. All state variables of the grid model also include all capacitor voltages and load voltages, but these variables show a stronger correlation with system stability compared to the state variables of branch currents.

to an output filter. The stability analysis of the TS model is performed using a quadratic Lyapunov candidate function. Paper [7] proposes a practical Lyapunov-based genetic algorithm for the estimation of ROA in electric power distribution systems. It utilizes a genetic algorithm to optimize the size of the estimated ROA by searching a proper Lyapunov function. However, the computational cost may burden the algorithm when the considered Lyapunov function is of high complexity. Papers [8] and [9] estimate the ROA of a DC-link motor drive and a synchronous generator, respectively, using the reverse trajectory principle. An approximate reverse system is proposed, and then the backward iteration on this system is performed from the boundary of an initially estimated domain of stability to a larger ROA. However, the approximation inverting the recurrent state functions may lose the generality of the original model. Additionally, this method becomes more difficult to implement for higher-dimension systems and does not give the closed-form equation of ROA. In paper [10], a novel method using the generalization of energy methods for assessment of the transient stability of a system with strong nonlinearity is proposed. The stability assessment is constructed via a sequence of convex optimization problems that are tractable even for large-scale dynamic systems. In addition, our previous study in [11] discusses the defects of the well-known Brayton-Moser mixed potential theory [12] and then develops a comprehensive approach to evaluate the large-signal stability in DC power grids. The proposed stability condition consists of grid parameters such as line impedance, capacitance, and inductance. It is worth mentioning that the set constructed by the proposed stability condition in [11] is different from the ROA. In terms of DC power grids, the ROA refers to a space of operating states (such as bus voltages, branch currents) that can converge to a steady-state equilibrium, from the perspective of controlled dynamic systems. Furthermore, the sum of squares (SOS) technique using a polynomial Lyapunov function in control system analysis is promising for global stability [13]–[15]. Paper [16] outlines a stability analysis approach based on a polynomial Lyapunov function, which is determined using the SOS technique to maximize the ROA of an equilibrium solution. In paper [17], the authors propose a SOS methodology for stability analysis and ROA estimation for nonlinear systems represented by polynomial fuzzy models via piecewise polynomial Lyapunov functions.

Nevertheless, these approaches may not be tractable for dealing with the characteristics of the potential functions in large-scale DC power grids with multiple CPLs. The SOS techniques for ROA estimation usually deal with polynomial systems. The approximation of nonpolynomial systems to polynomial systems may lead to modeling inaccuracy and high computational cost. Paper [18] investigates the Lyapunov stability of a bidirectional power converter feeding a single CPL. The stability analysis is based on a SOS programming method and an approximation of the converter system. However, the idea in [18] is hard to tailor to fit large-scale DC power grids due to the complicated dynamics and the curse of dimensionality in complex systems.

In a nutshell, large-signal stability analysis and ROA estimation of DC power grids are still open problems. This paper presents for the first time a rigorous approach to solve this problem. The main contributions of this paper can be summarized as follows:

First, we develop a novel approach to ROA estimation with less conservativeness, using a revised Brayton-Moser mixed potential theory. The approach tackles the common conflict between model accuracy of ROA estimation and computational overhead.

Second, this paper reveals the weak correlation between some state variables and system stability. It makes it possible to reduce computational cost and lessen the curse of dimensionality by separating these state variables.

Third, we carry out a comparison between the proposed novel ROA estimation approach and a traditional Lyapunov-based ROA estimation method. Our case study shows that the proposed approach can obtain a much less conservative ROA compared to the traditional method solving Lyapunov equations directly.

The structure of this paper is organized as follows: In section II and section III, the modeling of DC microgrids with multiple sources, converters, and CPLs is described and the necessary stability descriptions are discussed. In section IV, we study the DC microgrids model in a steady state and formulate an equilibrium analysis using a potential-based approach. We also point out several misunderstandings of the conventional potential theory. In Section V, we present the ROA estimation techniques of the DC microgrids model. Section VI substantiates our theoretical work through a case study.

II. DC Microgrids Modeling & Problem Formulation

A. The General Framework of DC Microgrids

A generalized circuit framework of a DC microgrid with multiple power converters and CPLs is described in Fig. 1.

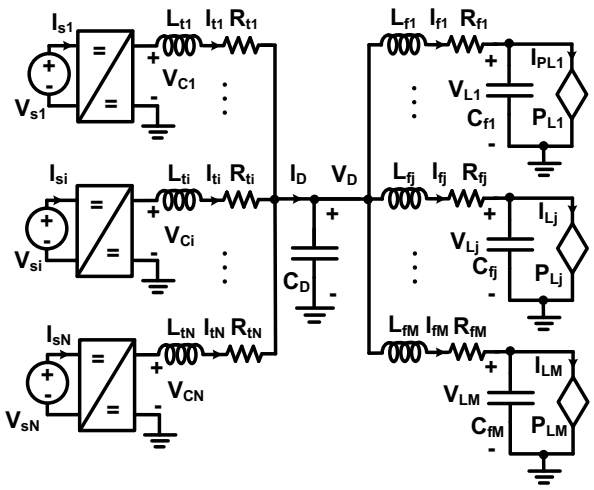

Fig. 1. The circuit structure of a typical DC microgrid.

Without loss of generality, we make the following assumptions about the circuit diagram of typical DC microgrids:

1) The power supplies are all constant-voltage sources.
2) The DC-DC power converters are deployed to step up or step down the voltage outputs. They can be ideal buck converters, boost converters, or buck-boost converters. No parasitic resistance or parasitic capacitance is considered.
3) The transmission lines are considered as impedances.
4) The demand side is composed of multiple CPLs. The CPL model is shown in Fig. 2(a), described by the following function:

This article has been accepted for publication in a future issue of this journal, but has not been fully edited. Content may change prior to final publication. Citation information: DOI 10.1109/TSG.2021.3081573, IEEE Transactions on Smart Grid

$$\begin{cases} I_{PL} = I_{max}, & V_L \le V_{min} \\ V_L = P_L/I_{PL}, & V_{min} \le V_L \le V_{max} \\ V_L = V_{max}, & I_{PL} < I_{min} \end{cases} \quad (1)$$

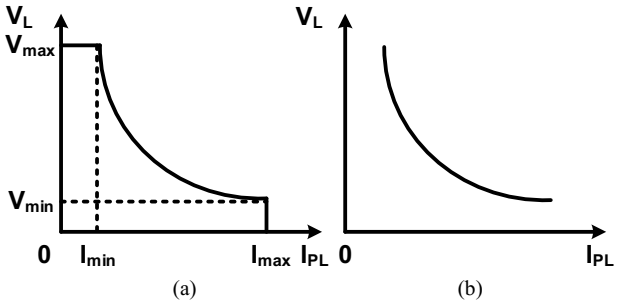

(a) (b)

Fig. 2. The CPL model: (a) the realistic model with operational bounds; (b) the traditional model without operational bounds.

In the existing literature on stability analysis of DC microgrids, the conventional modeling of CPLs does not consider operational bounds such as current limits or voltage limits, which is shown in Fig. 2(b). The traditional CPL model is not suitable for potential-based large-signal stability analysis due to violation of the prerequisites of potential theory. One prerequisite is that the domain of the studied dynamic model needs to be a *compact positively invariant set*; another prerequisite is that the studied model should be continuous and differentiable [19]. These prerequisites are not satisfied in the traditional CPL model. Alternatively, the CPL model in Fig. 2(a) indicates the operational upper bounds on load voltage and current, considering the practical conditions of CPLs in power grids. Having operational bounds is an *intrinsic* property of the CPL model. From the perspective of circuit characteristics, a parallel diode of CPL can be used to clamp the load voltage no smaller than the minimum voltage V_{min} ($V_{min} > 0$). This CPL model satisfies the prerequisites of the potential theory mentioned above.

B. Microgrids Model with Closed-Loop Converter Controllers

The proposed ROA estimation approach supports the utilization of several common controllers for power converters, such as traditional droop controllers, lag compensators, and lead compensators. The design of converter controllers can smooth the power flow and improve the quality of electric power through the regulation of output voltage. In our paper [11], we propose and validate a novel type of converter controller, called the droop-inertia controller, which generalizes better characteristics than the traditional droop controller in terms of control error and stability. The reason we set a traditional droop controller as the benchmark is that it is often utilized in existing microgrids with distributed control. However, the traditional droop controller has to compromise between large control error and weak stability: the traditional droop controller with larger resistance generates large steady-state control error, while the traditional droop controller with smaller resistance leads to larger oscillation and weak stability. In contrast, the proposed droop-inertia controller can ensure both smaller control error and smaller oscillation because of its higher degree of control, which shows the superiority of the proposed novel controller. Besides the better performance of the droop-inertia controller, the similarity in the structure between the novel controller and the droop controller also makes it more convenient and promising to be developed in DC microgrids in practice.

The circuit diagram of a power converter with a droop-inertia controller is described in Fig. 3. The proposed droop-inertia controller is intended to regulate the output voltage V_{Ci} to an expected value V_{refi} through the switching of I_{si}, which is a type of current control.

The transfer function of the droop-inertia controller can be obtained from its equivalent circuit, shown in Fig. 4, which is shown as follows:

$$G(s) = \frac{I_{si}(s)}{V_{refi}(s) - V_{Ci}(s)} = Y_{in}(s) = \frac{R_{pi} + sL_{qi} + R_{qi}}{R_{pi}(sL_{qi} + R_{qi})} \quad (2)$$

where Y_{in} is the equivalent admittance of the block in Fig. 4.

Therefore, we can develop the equivalent circuit structure of the microgrid model in Fig. 1, which is depicted in Fig. 5.

Notably, the droop-inertia controller can be downgraded to a PI controller by setting $R_{qi} = 0$ if needed. However, although a PI controller can ensure a zero steady-state error, it cannot realize the regulation of the power output of power sources, which is very critical in the operation of microgrids.

The current controller is designed to control the output voltage of the switching power converter. The idea behind the current-mode control is to build a voltage-controlled current source. Then the output of the current source is modulated to guarantee a constant output voltage from the power converter with changing load current. This idea is implemented through the collaboration of a current control loop and a voltage loop. The current control loop (inner loop) monitors the inductor current and builds the voltage-controlled current source. The voltage loop (outer loop) monitors the converter's output voltage and compiles the controlled current source to regulate the output voltage of the power converter.

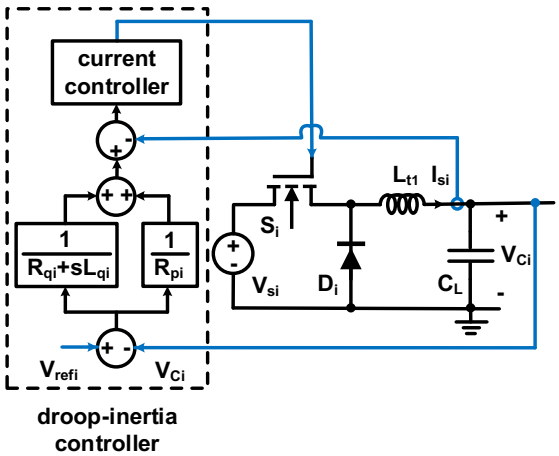

Fig. 3. The circuit diagram of a power converter with a droop-inertia controller.

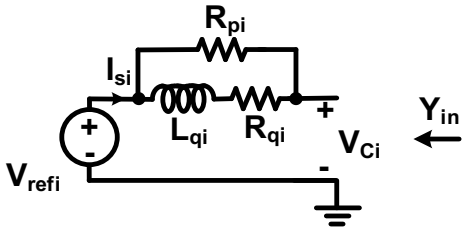

Fig. 4. The equivalent circuit of the proposed converter controller.

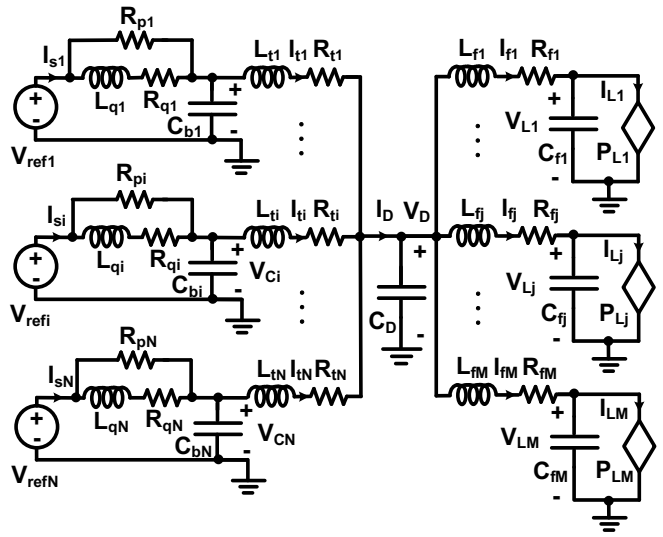

Fig. 5. The equivalent model of a DC microgrid under current-mode control.

III. Large-Signal Stability Analysis using Potential Functions

The Brayton-Moser mixed potential theory provides basic rigorous derivatives for large-signal stability analysis in nonlinear circuits [12]. In our paper [11], we dig into this theory more deeply and reveal its insufficiencies and flaws. In this section, we reintroduce the revised potential theory with our supplemental studies.

Specifically, our supplemental studies indicate the following three conclusions on the potential-based stability analysis:

1) We derive a more comprehensive analysis of the stability condition based on the original potential theory.

2) We realize the restriction of the prerequisite of the LaSalle theorem [19], which is ignored in the original potential theory. In fact, the conventional CPL model without operational bounds violates the prerequisite of the LaSalle theorem. It is necessary to pay attention to the boundary issues in the modeling of electric devices. The modified CPL model with operational bounds is an illustrative example.

3) We work on an accurate definition of large-signal stability, especially with consideration of multiple equilibrium points, which is not mentioned in the original potential theory.

Definition (Potential function [12]**):** Suppose there are r inductors, s capacitors, and b nonlinear resistors and power supplies in total in a circuit system. The components are sequentially numbered by μ starting from inductors and capacitors to resistors and power supplies. The potential function $P(i,v)$ of a circuit system is calculated as follows:

$$P(i,v)=\sum_{\mu=r+1}^{r+s} v_\mu i_\mu|_\Gamma+\sum_{\mu>r+s}^{r+s+b}\int_\Gamma v_\mu di_\mu \tag{3}$$

where v_μ and i_μ are element voltage and current, respectively. Regarding the notations of the elements, $1,2,\dots,r$ represent inductors; $r+1,\dots,r+s$ represent capacitors; $r+s+1,\dots,r+s+b$ represent nonlinear resistors and power sources. The integral term is also defined as voltage potential.

Additionally, there are several fundamental properties of the potential theory that have often been misconceived in previous studies.

1) *The potential theory supports stability analysis in autonomous systems only.* The potential theory is not appliable to time-variant systems, i.e., non-autonomous systems. This is restricted by the LaSalle stability theorem [19], which provides a theoretical foundation for the potential theory.

2) *The potential function of circuits depends only on the starting point and end point of the motion trajectory, independent of the trajectory itself.* This characteristic is the same as gravitational potential.

3) *The potential function is not a Lyapunov function or an energy function.* Non-negativity is a necessary condition of being a Lyapunov function or an energy function. Nevertheless, the potential function could be negative based on its definition. Assume a nonlinear element with the voltage potential $\eta=\int_0^{i_1} v_\mu di_\mu$. The dual function of the voltage potential is $\zeta=\int_0^{v_1} i_\mu dv_\mu$, also called current potential. The voltage potential and current potential are visualized in Fig. 6. Considering that the unit of the circuit potential is power, we can calculate the total power dissipation of the element, notated by Ψ.

$$\Psi=i_1v_1=\int_0^{i_1} v_\mu di_\mu+\int_0^{v_1} i_\mu dv_\mu=\eta+\zeta \tag{4}$$

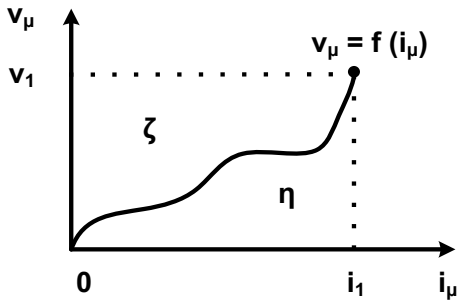

Fig. 6. Potential functions of a nonlinear element.

Considering that there are N source branches and M load branches, the potential function of the microgrid model in Fig. 5 is shown as follows.

$$\begin{aligned}P(i,v)=&\sum_{i=1}^{N}V_{refi}\left(I_{pi}+I_{qi}\right)-\frac{1}{2}\sum_{i=1}^{N}R_{pi}{I_{pi}}^2-\frac{1}{2}\sum_{i=1}^{N}R_{qi}{I_{qi}}^2\\&-\frac{1}{2}\sum_{i=1}^{N}R_{ti}{I_{ti}}^2-\frac{1}{2}\sum_{j=1}^{M}R_{fj}{I_{fj}}^2-\sum_{i=1}^{N}V_{Ci}\left(I_{pi}+I_{qi}-I_{ti}\right)\\&-V_D\left(\sum_{i=1}^{N}I_{ti}-\sum_{j=1}^{M}I_{fj}\right)+\sum_{j=1}^{M}Z_j\end{aligned} \tag{5}$$

where

$$Z_j=\begin{cases}\int_{V_{\min\_j}}^{V_{Lj}}\frac{P_{Lj}}{v}dv-P_{Lj}-V_{Lj}(I_{fj}-I_{Lj}),V_{Lj}>V_{\min\_j}\\I_{\max\_j}\left(V_{Lj}-V_{\min\_j}\right)-P_{Lj}-V_{Lj}(I_{fj}-I_{\max\_j}),V_{Lj}\le V_{\min\_j}\end{cases} \tag{6}$$

I_{pi} and I_{qi} are the currents through resistors R_{pi} and R_{qi}, respectively. $V_{\min\_j}$ is the lower bound of output voltage of the j-

This article has been accepted for publication in a future issue of this journal, but has not been fully edited. Content may change prior to final publication. Citation information: DOI 10.1109/TSG.2021.3081573, IEEE Transactions on Smart Grid

th CPL and $I_{\max\_j}$ is the upper bound of the current of the j-th CPL, as shown in Fig. 2(a). Other notations correspond to those marked in Fig. 5.

IV. ROA Estimation Using Potential Theory

In this section, we utilize the linearization of the nonlinear microgrid model to find a Lyapunov function to facilitate the ROA estimation. It is worth mentioning that this does not mean that the stability analysis is a small-signal analysis.

In terms of circuit analysis, *small-signal* stability analysis refers to the circuit stability subject to *sufficient* small disturbances. Small-signal stability analysis often utilizes classical eigenvalues or impedance techniques, where the stability is strictly defined as follows. In a continuous time-invariant dynamic model, $\dot{x} = f(x)$, an equilibrium state x_e is stable if there is an $\varepsilon_0 > 0$ with the following property: For all $\varepsilon_1, 0 < \varepsilon_1 < \varepsilon_0$, there is an $\varepsilon > 0$ such that if $\|x_e - x(t_0)\| < \varepsilon$, then $\|x_e - x(t)\| < \varepsilon_1$ for all $t > t_0$. This definition indicates that the equilibrium state x_e will be stable if the trajectory $x(t)(t > t_0)$ never leaves the ε_1-neighborhood of x_e, given the initial state $x(t_0)$ in a ε-neighborhood. From the definition of neighborhood, the area of the neighborhood of radius ε is sufficient small, which means that the ROA based on small-signal stability practically does not exist. In other words, small-signal stability analysis does not characterize the boundary of the asymptotic stability region. We cannot estimate the ROA of microgrid systems using small-signal stability analysis.

In this manuscript, we estimate the ROA of each stable equilibrium of the microgrid model using a Lyapunov function. Because the proposed approach can characterize the boundary of the asymptotic stability region for the system, it belongs to the scope of large-signal stability analysis.

Moreover, we would like to clarify some related concepts about stability analysis here.

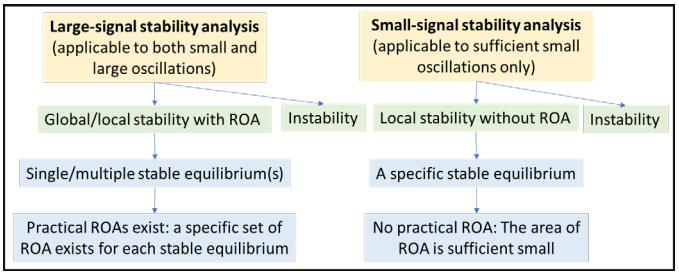

Fig. 7. The relationships among different types of stability.

From the perspective of circuit control, stability analysis can be classified into large-signal stability analysis and small-signal stability analysis. Large-signal stability analysis does not require the disturbances of the targeted system to be sufficient small; small-signal stability analysis is applicable *only* to systems with sufficient small disturbances. With large-signal stability analysis, we can know whether a microgrid system is globally stable, locally stable, or unstable. Global stability and local stability can be checked by finding a Lyapunov function that is positive definite with a negative definite time derivative. A locally stable system determined by large-signal stability analysis has a "practical" ROA, that is, the area of ROA is not sufficient small. With small-signal stability analysis, we can determine whether a microgrid system is locally stable or unstable. It is worth mentioning that a local stable system determined by small-signal stability analysis does not have a "practical" ROA, that is, the area of ROA is sufficient small. Therefore, we cannot estimate the ROA of microgrid systems using small-signal stability analysis.

The approach of ROA estimation is investigated in section IV and section V. The general procedure is visualized in the following flowchart, where the formulas and notations are explained in detail in the following sections.

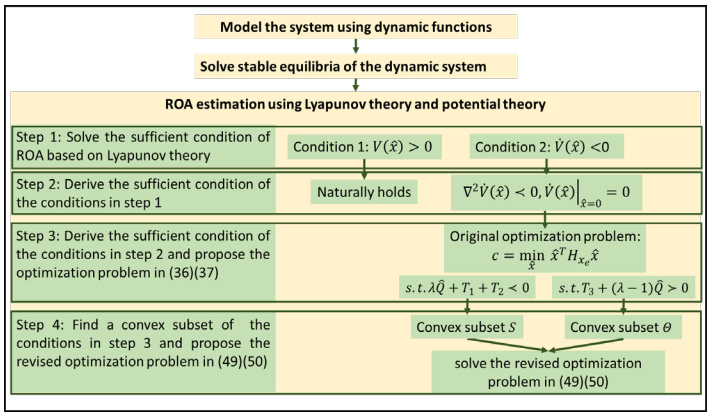

Fig. 8. The flowchart of the ROA estimation.

A. Problem Formulation

In potential theory, the dynamic equation of the model in Fig. 5 can be described as follows:

$$-J\frac{dx}{dt} = \frac{\partial P(x)}{\partial x} \tag{7}$$

where $x = [i \ v]^T$, $J = diag\{[-L \quad C]\}$, and L and C are the diagonal inductance matrix and the diagonal capacitance matrix, respectively. i and v are the current vector and the voltage vector, respectively.

$i = [I_{p1}, I_{p2}, \dots, I_{pN}, I_{q1}, I_{q2}, \dots, I_{qN}, I_{t1}, I_{t2}, \dots, I_{tN}, I_{f1}, \dots, I_{fM}]$,

$v = [V_{C1}, \dots, V_{CN}, V_D, V_{L1}, \dots, V_{LM}]$.

Nevertheless, whether J is positive definite (p.d.) is highly dependent on the values of L and C under this description. Hence, another expression of this system is proposed and preferred, which considers (P^*, J^*) instead of (P, J), such that

$$-J^*\frac{dx}{dt} = \nabla P^*(x) \tag{8}$$

where

$$J^* = \left(\lambda\mathbb{I} + \frac{\partial^2 P(x)}{\partial x^2}\mathcal{M}\right)\cdot J, P^* = \lambda P + \frac{1}{2}\left(\frac{\partial P(x)}{\partial x}, \mathcal{M}\frac{\partial P(x)}{\partial x}\right) \tag{9}$$

where $\mathbb{I}$ is the identity matrix, $\mathcal{M}$ can be any constant symmetric matrix, and λ can be any constant. Under this description, J^* is always positive definite in stable dynamic systems. ∇ represents the gradient operator.

The following Theorem 1 provides accurate stability information for each equilibrium point of the microgrid model. The theorem investigates sufficient conditions for the large-signal stability of equilibrium points and shows the sufficient conditions for the existence of a Lyapunov function at equilibrium points, which facilities the ROA estimation.

This article has been accepted for publication in a future issue of this journal, but has not been fully edited. Content may change prior to final publication. Citation information: DOI 10.1109/TSG.2021.3081573, IEEE Transactions on Smart Grid

Theorem 1: Given a nonlinear circuit $\frac{dx}{dt} = f(x)$, as shown in Fig. 5, the potential-based dynamic function of the circuit is $-J^* \frac{dx}{dt} = \frac{\partial P^*(x)}{\partial x}$. Let $f: \mathcal{R}^n \to \mathcal{R}$ be a C^1 function and $P^*: \mathcal{R}^n \to \mathcal{R}$ be a C^2 function. Suppose D is a neighborhood of equilibrium point x_e. If $J^* \succ 0$, $H(P^*)|_{x=x_e} \succ 0$, $P^*(x)$ is radially unbounded and all equilibrium points of the system form a compact set, then $x = x_e$ is a stable equilibrium point and there exists a Lyapunov function at $x = x_e$.

The proof is presented in Appendix A.

Suppose an equilibrium point $x = x_e$ of the microgrid model with the dynamics that satisfies the conditions mentioned in Theorem 1. Then we can construct a Lyapunov function at the equilibrium point $x = x_e$ according to the following Theorem 2.

Theorem 2: Given a nonlinear circuit $\frac{dx}{dt} = f(x)$, as shown in Fig. 5, the potential-based dynamic function of the circuit is $-J^* \frac{dx}{dt} = \frac{\partial P^*(x)}{\partial x}$. Suppose $J^* \succ 0$, $H(P^*)|_{x=x_e} \succ 0$, where x_e is an equilibrium point of the system. Then a Lyapunov function at $x = x_e$ can be constructed as follows:

$$V(\hat{x}) = \hat{x}^T H(P^*)|_{x=x_e} \hat{x} = \hat{x}^T H_{x_e} \hat{x}, \quad (10)$$

where $\hat{x} = x - x_e, H(P^*)|_{x=x_e}$ is the Hessian matrix of the potential function $P^*(x)$ at $x = x_e$; $H(P^*)|_{x=x_e}$ is also shortened as H_{x_e}.

Proof: In Appendix A, the dynamic model is linearized as follows:

$$\dot{\hat{x}} = A\hat{x} \quad (11)$$

where $A = -(J^*)^{-1} H_{x_e}$.

Consider the Lyapunov equation corresponding to the Lyapunov function $L(x)$:

$$A^T \mathcal{N} + \mathcal{N} A = -Q \quad (12)$$

where $\mathcal{N} = H_{x_e}$. Then we will prove $Q \succ 0, Q = Q^T$.

1) $Q \succ 0$: Considering that H_{x_e} is symmetric, we have

$$\begin{aligned} A^T \mathcal{N} + \mathcal{N} A &= -{H_{x_e}}^T ((J^*)^{-1})^T H_{x_e} - H_{x_e} (J^*)^{-1} H_{x_e} \\ &= -H_{x_e} \cdot (((J^*)^{-1})^T + (J^*)^{-1}) \cdot H_{x_e} \end{aligned} \quad (13)$$

Lemma: For $J^* \succ 0$, $J^* \in \mathcal{R}^{n \times n}$, $(J^*)^T$ and $(J^*)^{-1}$ are also positive definite. Hence, we have $(J^*)^{-1} \succ 0, ((J^*)^{-1})^T \succ 0$.

Given any vector $y \neq 0$, we have:

$$\begin{aligned} & y^T (J^*)^{-1} y > 0, y^T ((J^*)^{-1})^T y > 0 \\ \Rightarrow\ & y^T \cdot ((J^*)^{-1} + ((J^*)^{-1})^T) \cdot y > 0 \end{aligned} \quad (14)$$

which means $(J^*)^{-1} + ((J^*)^{-1})^T \succ 0$.

Denote $S = (J^*)^{-1} + ((J^*)^{-1})^T \succ 0$.

$$\begin{aligned} y^T (A^T \mathcal{N} + \mathcal{N} A) y &= y^T \cdot \{-H_{x_e} \cdot S \cdot H_{x_e}\} \cdot y \\ &= -(H_{x_e} y)^T \cdot S \cdot H_{x_e} y \end{aligned} \quad (15)$$

Since H_{x_e} is a symmetric and positive definite matrix, H_{x_e} has full rank. So $H_{x_e} y \neq 0\ \forall y \neq 0$. Considering $S \succ 0$, we have

$$-(H_{x_e} y)^T \cdot S \cdot H_{x_e} y < 0 \Rightarrow A^T \mathcal{N} + \mathcal{N} A = -Q \prec 0 \Rightarrow Q \succ 0 \quad (16)$$

2) $Q = Q^T$: Because $\mathcal{N} = H_{x_e}$, we have $\mathcal{N} = \mathcal{N}^T$. Hence,

$$Q^T = -\mathcal{N}^T A - A^T \mathcal{N}^T = -\mathcal{N} A - A^T \mathcal{N} = Q \quad (17)$$

Conclusion: From $Q \succ 0$ and $Q = Q^T$, we can conclude that $L(x) = \hat{x}^T H_{x_e} \hat{x}$ is a Lyapunov function at $x = x_e$.

Theorem 2 rigorously derives a Lyapunov function for the microgrid system in Fig. 5. With the potential-based modeling of the microgrid system, we can directly use $H(P^*)|_{x=x_e}$ to construct a Lyapunov function. This technique reduces the computational cost of solving a Lyapunov equation in the traditional ROA estimation approach. In the traditional approach, it is necessary to solve the Lyapunov equation $A^T \mathcal{N} + \mathcal{N} A = -Q$ to obtain the Lyapunov function in the form of $L(\hat{x}) = \hat{x}^T \mathcal{N} \hat{x}$. Matrix Q is supposed as an arbitrary real symmetric and positive definite matrix (usually Q is supposed as an identity matrix). The Hessenberg-Schur algorithm is often utilized to solve Lyapunov equations, which has a high computational cost.

In a dynamic system, the ROA can be estimated by finding a Lyapunov function that is positive definite with time derivative negative definite. In other words, the estimated ROA is the set where the following conditions are satisfied:

$$\begin{cases} V(\hat{x}) > 0 \\ \dot{V}(\hat{x}) < 0 \end{cases} \quad (18)$$

Considering that $V(\hat{x}) > 0$ always holds, the ROA can be estimated as the solution of $\dot{V}(\hat{x}) < 0$. However, the calculation is not simple, especially when the microgrid system is one with high dimensionality. In the following section B and section C, we present how to solve this condition with less computational burden.

B. Sufficient Condition of $\dot{V}(\hat{x}) < 0$

At the end of the above section, there are two conditions to estimate the ROA. Since $H_{x_e} \succ 0$, $V(\hat{x}) = \hat{x}^T H_{x_e} \hat{x} > 0$ always holds. Therefore, we only need to solve $\dot{V}(\hat{x}) < 0$ with the potential-based modeling of microgrid dynamics. In this section, we propose a novel approach to solve the condition $\dot{V}(\hat{x}) < 0$. The solution of $\dot{V}(\hat{x}) < 0$ can be seen as the estimated ROA for stable equilibrium points.

First, we have the following sufficient condition to guarantee $\dot{V}(\hat{x}) < 0$:

$$\begin{cases} \nabla^2 \dot{V}(\hat{x}) \prec 0 \\ \dot{V}(\hat{x})\big|_{\hat{x}=0} = 0 \end{cases} \quad (19)$$

Hence, we aim to solve the above two conditions next.

The nonlinear circuit shown in Fig. 5 can be described by $\frac{dx}{dt} = f(x)$ or $-J^* \frac{dx}{dt} = \frac{\partial P^*(x)}{\partial x}$. The first equation is a common expression of the dynamic function, and the second function is the dynamic function constructed from the perspective of potential theory. Consider the first dynamic function

$$\dot{x} = f(x) \quad (20)$$

Linearizing the system at equilibrium $x = x_e$, we have

$$\begin{aligned} \dot{\hat{x}} &= f(x_e + \hat{x}) \\ &= \nabla f(x_e)\hat{x} + f(x_e + \hat{x}) - \nabla f(x_e)\hat{x} \end{aligned} \quad (21)$$

where $\hat{x} = x - x_e$.

Considering the equivalence of the two different dynamic functions, we have

$$\frac{dx}{dt} = -(J^*)^{-1} \nabla P^*(x) = f(x) \quad (22)$$

Hence, we have $A = -(J^*)^{-1} H_{x_e} = \nabla f(x_e)$. The first equality holds due to the definition of the matrix A in the proof of Theorem 2. Then we obtain the linearized system:

$$\dot{\hat{x}} = A\hat{x} \tag{23}$$

Moreover, define the residual term as follows:

$$g(\hat{x}) = f(x_e + \hat{x}) - \nabla f(x_e)\hat{x} \tag{24}$$

Plugging the dynamic functions with all circuit variables into the residual function $g(\hat{x})$, we obtain

$$g(\hat{x}) = [0_{1\times(4N+M+1)}, \Phi(\hat{V}_L)_{1\times M}]^T \tag{25}$$

where $\Phi(\hat{V}_L) = [\varphi_1(\hat{v}_{L1}), \dots, \varphi_M(\hat{v}_{LM})]$. It is worth mentioning that the non-zero elements of $g(\hat{x})$ correspond to M load voltages only; the other elements of $g(\hat{x})$ corresponding to other state variables are all zero. We label the load voltages as the state variables showing strong relationships to system stability; state variables other than load voltages are labeled as those showing weak relationships to system stability.

Considering the dynamics of circuit elements, we obtain

$$\varphi_j(\hat{v}_j) = -\frac{P_{Lj}}{C_{fj}}\frac{{\hat{v}_j}^2}{(v_j{}^* + \hat{v}_j){v_j}^{*2}} \tag{26}$$

and

$$\varphi_j{}'(\hat{v}_j) = -\frac{P_{Lj}}{C_{fj}{v_j}^{*2}}\left(1 - \frac{{v_j}^{*2}}{(v_j{}^* + \hat{v}_j)^2}\right) \tag{27}$$

where $j \in \{1,2,\dots,M\}$.

Then we calculate the derivative of the Lyapunov function $V(\hat{x})$ as follows:

$$\begin{aligned}\dot{V}(\hat{x}) &= \dot{\hat{x}}^T H_{x_e}\hat{x} + \hat{x}^T H_{x_e}\dot{\hat{x}}\\ &= f(x_e+\hat{x})^T H_{x_e}\hat{x} + \hat{x}^T H_{x_e} f(x_e+\hat{x})\\ &= [\nabla f(x_e)\hat{x} + g(\hat{x})]^T H_{x_e}\hat{x} + \hat{x}^T H_{x_e}[\nabla f(x_e)\hat{x} + g(\hat{x})]\\ &= \hat{x}^T\left[\nabla f^T(x_e)H_{x_e} + H_{x_e}\nabla f(x_e)\right]\hat{x} + 2\hat{x}^T H_{x_e} g(\hat{x})\end{aligned} \tag{28}$$

Considering the equivalence of the two different dynamic functions, we have

$$\begin{aligned}&\nabla f^T(x_e)H_{x_e} + H_{x_e}\nabla f(x_e)\\ &= -\nabla^T\left((J^*)^{-1}\nabla P^*(x_e)\right)H_{x_e} - H_{x_e}\nabla\left((J^*)^{-1}\nabla P^*(x_e)\right)\\ &= -{H_{x_e}}^T((J^*)^{-1})^T H_{x_e} - H_{x_e}(J^*)^{-1}H_{x_e}\\ &= -Q \prec 0\end{aligned} \tag{29}$$

where Q is firstly defined in the proof of Theorem 2.

Suppose

$$Q = -\begin{bmatrix} Q_{11} & Q_{12}\\ Q_{21} & \hat{Q}\end{bmatrix}, H_{x_e} = \begin{bmatrix} H_{11} & H_{12}\\ H_{21} & \hat{H}\end{bmatrix} \tag{30}$$

where $Q_{11} \in \mathcal{R}^{(4N+M+1)\times(4N+M+1)}$,
$H_{11} \in \mathcal{R}^{(4N+M+1)\times(4N+M+1)}, \hat{Q} \in \mathcal{R}^{M\times M}, \hat{H} \in \mathcal{R}^{M\times M}$.

Denote $\hat{x} = [{\hat{x}_a}^T, {\hat{V}_L}^T]^T$, where $V_L = [V_{L1}, \dots, V_{LM}]$, $x_a = [I_{p1}, \dots, I_{pN}, I_{q1}, \dots, I_{qN}, I_{t1}, \dots, I_{tN}, I_{f1}, \dots, I_{fM}, V_{C1}, \dots, V_{CN}, V_D]$.

Then the Hessian of $\dot{V}(\hat{x})$ can be calculated as follows:

$$\nabla^2\dot{V}(\hat{x}) = \begin{bmatrix} Q_{11} & Q_{12} + 2H_{12}\nabla_c\Phi(\hat{V}_L)\\ Q_{21} + 2(H_{12}\nabla_c\Phi(\hat{V}_L))^T & \hat{Q} + 2\nabla^2\left(\hat{V}_L{}^T\hat{H}\Phi(\hat{V}_L)\right) + 2\hat{x}_a H_{12}{\nabla_c}^2\Phi(\hat{V}_L)\end{bmatrix} \tag{31}$$

where $\nabla_c\Phi(\hat{V}_L) = diag\{\nabla\varphi_1(\hat{v}_1), \dots, \nabla\varphi_M(\hat{v}_M)\}, {\nabla_c}^2\Phi(\hat{V}_L) = diag\{\nabla^2\varphi_1(\hat{v}_1), \dots, \nabla^2\varphi_M(\hat{v}_M)\}$.

The calculation is shown in Appendix B.

Formulating a transformation using the properties of the Schur complement, we have

$$\begin{aligned}&\nabla^2\dot{V}(\hat{x}) \prec 0\\ &\Leftrightarrow \hat{Q} + 2\nabla^2\left(\hat{V}_L{}^T\hat{H}\Phi(\hat{V}_L)\right) + 2\hat{x}_a H_{12}{\nabla_c}^2\Phi(\hat{V}_L)\\ &-\left(Q_{21} + 2\nabla_c\Phi(\hat{V}_L)H_{12}{}^T\right)Q_{11}{}^{-1}(Q_{12} + 2H_{12}\nabla_c\Phi(\hat{V}_L)) \prec 0\end{aligned} \tag{32}$$

Denote $T_1 \triangleq 2\nabla^2\left(\hat{V}_L{}^T\hat{H}\Phi(\hat{V}_L)\right), T_2 \triangleq 2\hat{x}_a H_{12}{\nabla_c}^2\Phi(\hat{V}_L), T_3 \triangleq \left(Q_{21} + 2\nabla_c\Phi(\hat{V}_L)H_{12}{}^T\right)Q_{11}{}^{-1}\left(Q_{12} + 2H_{12}\nabla_c\Phi(\hat{V}_L)\right)$.

Then we obtain

$$\nabla^2\dot{V}(\hat{x}) \prec 0 \Leftrightarrow \hat{Q} + T_1 + T_2 - T_3 \prec 0 \tag{33}$$

Given a proper $\lambda \in \mathcal{R}$, the above condition can be relaxed as follows:

$$\lambda\hat{Q} + T_1 + T_2 - (T_3 + (\lambda-1)\hat{Q}) \prec 0 \tag{34}$$

Then the sufficient condition of the above condition is as follows:

$$\begin{cases}\lambda\hat{Q} + T_1 + T_2 \prec 0\\ T_3 + (\lambda-1)\hat{Q} \succ 0\end{cases} \tag{35}$$

The derivation reduces the computational cost and lessens the curse of dimensionality, which enables our approach to fit for large-scale power grid models. It is noted that the computational dimension of the constraints in (35) is M^2, which is much lower than the dimension of the traditional ROA estimation method, i.e., $(4N+2M+1)^2$.

V. Convexity Analysis & Optimization Problem Formulation

Considering the sufficient condition of $\dot{V}(\hat{x}) < 0$ derived at the end of section IV, we can formulate an optimization problem to solve the boundary of ROA as follows:

$$c = \min_{\hat{x}}\ \hat{x}^T H_{x_e}\hat{x} \tag{36}$$

$$\text{s.t.}\ \begin{cases}\lambda\hat{Q} + T_1 + T_2 \prec 0\\ T_3 + (\lambda-1)\hat{Q} \succ 0\end{cases} \tag{37}$$

However, the feasible set may not be convex, which burdens the solving of the optimization problem. Therefore, it is essential to discuss the convexity of the feasible set before solving the optimization problem. In fact, the feasible set may not be convex according to our rigorous proof, which requires us to solve a convex subset of the feasible region. In this section, we present a discussion of the convexity of the feasible region of the optimization problem, which is constructed by the constraints in (37).

A. Convexity of the first condition $\lambda\hat{Q} + T_1 + T_2 \prec 0$

In this part, we discuss the convexity of the solution of $\lambda\hat{Q} + T_1 + T_2 \prec 0$.

The term $\lambda\hat{Q} + T_1 + T_2$ is a diagonal matrix. Denote the diagonal elements by $f_{\mu i}(\hat{v}_i), i = 1, \dots, M$. Then the element is solved as follows:

$$\begin{aligned}&f_{\mu i}(\hat{v}_i)\\ &= \lambda\hat{Q}_i + 2\frac{d^2}{d{\hat{v}_i}^2}\left(-\frac{P_{Li}}{{v_i}^{*2}} + 2R_{fi}\right)\hat{v}_i\varphi_i(\hat{v}_i) + 2\frac{d^2}{d{\hat{v}_i}^2}\varphi_i(\hat{v}_i)\left(\hat{I}_{fi} - \hat{v}_T R_{fi}\right)\\ &= {K_0}^i + \sigma''\left({K_1}^i\hat{v}_i + 2{K_2}^i L_1(\hat{I}_{fi}, \hat{v}_T)\right) + 2{K_1}^i\sigma'\end{aligned} \tag{38}$$

where ${K_0}^i = \lambda\hat{Q}_i, {K_1}^i = 2\left(-\frac{P_{Li}}{{v_i}^{*2}} + 2R_{fi}\right)\left(-\frac{P_{Li}}{C_{Li}}\frac{1}{{v_i}^{*2}}\right), {K_2}^i = -\frac{P_{Li}}{C_{Li}}\frac{1}{{v_i}^{*2}}, L_1(\hat{I}_{fi}, \hat{v}_T) = \hat{I}_{fi} - \hat{v}_T R_{fi}, \sigma(\hat{v}_i) = \frac{{\hat{v}_i}^2}{{v_i}^* + \hat{v}_i}$.

This article has been accepted for publication in a future issue of this journal, but has not been fully edited. Content may change prior to final publication. Citation information: DOI 10.1109/TSG.2021.3081573, IEEE Transactions on Smart Grid

Next, we discuss the convexity of $\lambda\hat{Q}+T_1+T_2\prec 0$ by categorized discussion.

(a) $2K_1{}^i+K_0{}^i\geq 0$:

In this case, it can be proved that the solution of $f_{\mu i}(\hat{v}_i)<0, i=1,2,\dots,M$ is convex. The proof is shown in Appendix C.

(b) $2K_1{}^i+K_0{}^i<0$:

In this case, the solution of $f_{\mu i}(\hat{v}_i)<0$ is not convex. We then need to find a convex subset of the solution that is as large as possible while decreasing the computational cost.

Assume $\hat{v}_i\geq\hat{v}_{i\_min}$. Linearize $g(\hat{v}_i,\hat{I}_{fi},\hat{v}_T)$ at $\hat{v}_i=\hat{v}_{i\_min}$:

$$L_3(\hat{v}_i,\hat{I}_{fi},\hat{v}_T)>\frac{1}{2{v_i}^{*2}}(2K_1{}^i+K_0{}^i)[({v_i}^*+\hat{v}_{i\_min})^3+3({v_i}^*+\hat{v}_{i\_min})^2(\hat{v}_i-\hat{v}_{i\_min})] \quad (39)$$

Therefore, we obtain a convex subset as follows:

$$L_3(\hat{v}_i,\hat{I}_{fi},\hat{v}_T)>\frac{1}{2{v_i}^{*2}}(2K_1{}^i+K_0{}^i)[({v_i}^*+\hat{v}_{i\_min})^3+3({v_i}^*+\hat{v}_{i\_min})^2(\hat{v}_i-\hat{v}_{i\_min})],(\hat{v}_i\geq\hat{v}_{i\_min}) \quad (40)$$

Combining case (a) with case (b), the convex subset of the solution of $\lambda\hat{Q}+T_1+T_2\prec 0$ is the intersection set of all convex sets/subsets corresponding to each load branch respectively as in the above discussion. For example, given a DC microgrid model, we first need to determine which category each load branch belongs to by calculating $2K_1{}^i+K_0{}^i$. If the result is non-negative, the solution of $f_{\mu i}(\hat{v}_i)<0$ is convex; if the result is negative, the solution of $f_{\mu i}(\hat{v}_i)<0$ is not convex, and hence we will find a convex subset using the above equation, where i represents the corresponding load branch. Next, we solve the intersection set of all convex sets/subsets obtained in the first step. Finally, we can get a convex subset of the solution of $\lambda\hat{Q}+T_1+T_2\prec 0$.

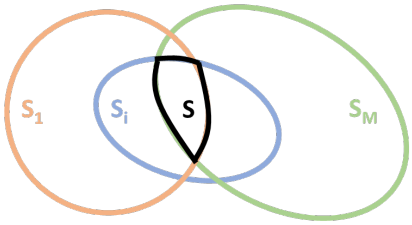

Fig. 9. Intersection set.

As visualized in Fig. 9, the convex subsets of $\lambda\hat{Q}+T_1+T_2\prec 0$ are $S=S_1\cap\cdots S_i\cap\cdots S_M$, where $S_1,\dots,S_i,\dots,S_M$ are the convex sets/subsets corresponding to each point of load (PoL), respectively, and can be solved by the above category discussion.

B. Convexity of the second condition $T_3+(\lambda-1)\hat{Q}\succ 0$

In this part, we discuss the convexity of the solution of $T_3+(\lambda-1)\hat{Q}\succ 0$.

Considering

$$T_3\triangleq\left(Q_{21}+2\nabla_c\Phi(\hat{V}_L){H_{12}}^T\right){Q_{11}}^{-1}\left(Q_{12}+2H_{12}\nabla_c\Phi(\hat{V}_L)\right) \quad (41)$$

we can formulate a transformation using the Schur complement as follows:

$$T_3+(\lambda-1)\hat{Q}\succ 0 \overset{Q_{11}\prec 0}{\Longleftrightarrow} X=\begin{bmatrix}Q_{11} & Q_{12}+2H_{12}\nabla_c\Phi(\hat{V}_L)\\ Q_{21}+2\nabla_c\Phi(\hat{V}_L){H_{12}}^T & (1-\lambda)\hat{Q}\end{bmatrix}\prec 0 \quad (42)$$

where $\nabla_c\Phi(\hat{V}_L)=diag\{\nabla\varphi_1(\hat{v}_1),\dots,\nabla\varphi_M(\hat{v}_M)\}$.

In addition, we have already derived that

$${\varphi_i}'(\hat{v}_i)=-\frac{P_{Li}}{C_{fi}{v_i}^{*2}}\left(1-\frac{{v_i}^{*2}}{({v_i}^*+\hat{v}_i)^2}\right) \quad (43)$$

Theorem 3: Given the above definition of matrix X in (42), $X\prec 0$ is a linear matrix inequality (LMI) of $[\dots,\varphi_i'(\hat{v}_i),\dots]$, where $i\in\{1,2,\dots,M\}$.

Proof: we have

$$X=\begin{bmatrix}Q_{11} & Q_{12}\\ Q_{21} & (1-\lambda)\hat{Q}\end{bmatrix}+\begin{bmatrix}0 & 2H_{12}\nabla_c\Phi(\hat{V}_L)\\ 2\nabla_c\Phi(\hat{V}_L){H_{12}}^T & 0\end{bmatrix} \quad (44)$$

It can be written in the form of

$$X=A_0+A_1{\varphi_1}'(\hat{v}_1)+\cdots+A_M{\varphi_M}'(\hat{v}_M) \quad (45)$$

where $A_0,\dots,A_M$ are parameter matrices. Therefore, $X\prec 0$ is a linear matrix inequality (LMI) of $[\dots,\varphi_i'(\hat{v}_i),\dots]$, where $i\in\{1,2,\dots,M\}$.

From Theorem 3, we know that $X\prec 0$ is an LMI, which indicates that the solution of $X\prec 0$ is a convex set. However, the computational cost of brutally solving $X\prec 0$ is high because X is non-symmetric and high-dimensional. Considering $v_i={v_i}^*+\hat{v}_i>0$, ${\varphi_i}'(\hat{v}_i)$ is monotonic, we can therefore choose a convex subset Θ of the solution of $X\prec 0$ as follows to decrease the computational complexity:

$$\Theta: l_{bi}\leq\hat{v}_i\leq u_{bi},\forall i\in\{1,2,\dots,M\} \quad (46)$$

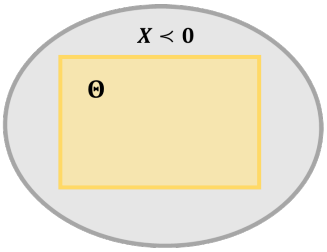

Fig. 10. The convex subset Θ.

C. Optimization problem formulation for ROA estimation

Review the optimization problem proposed at the beginning of section V.

$$c=\min_{\hat{x}}\ \hat{x}^T H_{x_e}\hat{x} \quad (47)$$

$$\text{s.t.}\ \begin{cases}\lambda\hat{Q}+T_1+T_2\prec 0\\ T_3+(\lambda-1)\hat{Q}\succ 0\end{cases} \quad (48)$$

Based on the above analysis, we know that the original feasible region constructed by the constraints is not convex, which burdens the solving of the optimization problem. Therefore, we find a convex subset of the original feasible region to estimate the ROA with less computational cost.

The convex subset of the original feasible region is solved as $\{S\cap\Theta\}$. Then the optimization problem to solve the ROA boundary can be revised as follows:

$$c=\min_{\hat{x}}\ \hat{x}^T H_{x_e}\hat{x} \quad (49)$$

$$\text{s.t.}\ \partial\{S\cap\Theta\} \quad (50)$$

It is worth mentioning that the revised feasible region is the *boundary* of set $\{S\cap\Theta\}$ instead of the set $\{S\cap\Theta\}$ itself, which is

This article has been accepted for publication in a future issue of this journal, but has not been fully edited. Content may change prior to final publication. Citation information: DOI 10.1109/TSG.2021.3081573, IEEE Transactions on Smart Grid

visualized as the black curve in Fig. 11. The ROA is estimated as $\{\Omega_c: \hat{x}^T H_{x_e} \hat{x} \le c\}$.

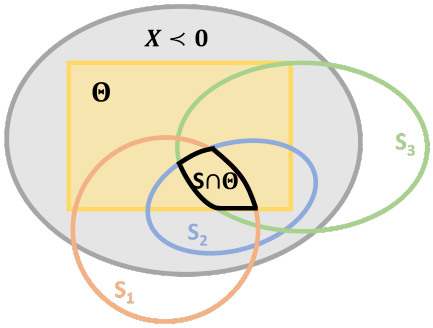

Fig. 11. The domain of the optimization problem.

Our following derivation leverages the characteristics of the two constraints in the optimization problem. The first constraint $\lambda\widehat{Q} + T_1 + T_2 \prec 0$ involves only *diagonal* matrices; the second constraint $T_3 + (\lambda - 1)\widehat{Q} \succ 0$ involves non-diagonal matrices but refers only to *load voltages* in all state variables. In our algorithm, we label the load voltages as the state variables showing strong relationships to system stability; state variables other than load voltages are labeled as those showing weak relationships to system stability. Separating the state variables with strong relationships from those with weak relationships can reduce computational cost and lessen the curse of dimensionality, which enables our approach to fit for large-scale power grid models.

In the proposed novel ROA estimation approach, there are multiple techniques applied to reduce the computational costs. We conclude the techniques and their influence on the computational costs and compare them with the traditional ROA estimation method. The comparison is visualized in the following table.

TABLE I. COMPARISON OF COMPUTATION COSTS BETWEEN DIFFERENT ROA ESTIMATION METHODS

Algorithm steps and computational cost	The traditional ROA estimation method	The proposed novel ROA estimation method
Step 1: solve the Lyapunov equation $A^T\mathcal{N} + \mathcal{N}A = -Q$ to determine the Lyapunov function $V(\hat{x}) = \hat{x}^T\mathcal{N}\hat{x}$	Given that Q is an identity matrix, solve the Lyapunov equation $A^T\mathcal{N} + \mathcal{N}A = -Q$.	No need to solve the Lyapunov equation. According to the proposed potential-based approach, we directly set $\mathcal{N} = H_{x_e}$.
Computational dimension of step 1	$(4N + 2M + 1)^2$	None
Step 2: solve the optimization problem to estimate ROA	$c = \min_{\hat{x}} \hat{x}^T\mathcal{N}\hat{x}$ s.t. $\begin{cases} V(\hat{x}) > 0 \\ \dot{V}(\hat{x}) < 0 \end{cases}$	$c = \min_{\hat{x}} \hat{x}^T H_{x_e}\hat{x}$ s.t. $\partial\{S \cap \Theta\}$
Computational dimension of step 2	The dimensions of the objective function and the constraints are all $(4N + 2M + 1)^2$.	The dimension of the objective function is $(4N + 2M + 1)^2$; the dimension of the constraint is M^2, based on the definition of set S and set Θ. Set S involves only *load voltages* in all state variables.

VI. CASE STUDY

In this case study, we investigate ROA estimation for a DC microgrid model with multiple CPLs to illustrate our proposed techniques.

The DC microgrid model is built as in Fig. 1 with $N = M = 2$, where N and M are the numbers of source branches and load branches, respectively. With the utilization of droop-inertia converter controllers, the equivalent circuit diagram of the grid model is depicted as follows:

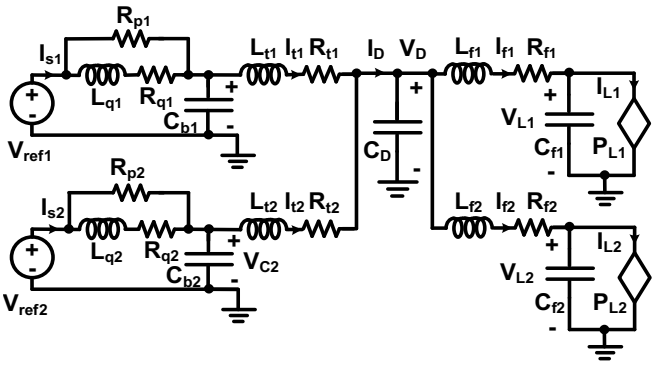

Fig. 12. The equivalent circuit diagram of the microgrid model.

The model parameters are shown in the following table:

TABLE II. SIMULATION PARAMETERS
(The unit: V, H, F, Ohm, W)

V_{ref1}	200	R_{p1}	5	R_{q1}	5	L_{q1}	0.1	C_{b1}	1
R_{t1}	8	L_{t1}	0.1	R_{f1}	5	L_{f1}	0.1	C_{f1}	1
V_{ref2}	200	R_{p2}	5	R_{q2}	5	L_{q2}	0.1	C_{b2}	1
R_{t2}	8	L_{t2}	0.1	R_{f2}	3	L_{f2}	0.1	C_{f2}	1
C_D	1	$I_{\max 1}$	∞	$V_{\min 1}$	0	$I_{\max 2}$	20	$V_{\min 2}$	20
P_{L1}	200	P_{L2}	400						

Given the parameter settings, load P_{L1} always works in constant power mode; load P_{L2} works in constant power mode only when the load voltage is higher than the voltage lower bound $V_{\min 2}$. Here, we estimate ROA for the stable equilibrium point(s) only when both CPLs work in constant power mode, which is the regular operating condition in power grids.

A. Steady-State Analysis of the Microgrid Model

In this section, we aim at solving the stable equilibrium point(s) of the given model. First, we solve the Thevenin equivalence of the model in steady-state. The circuit structure of the Thevenin equivalent circuit is shown as follows:

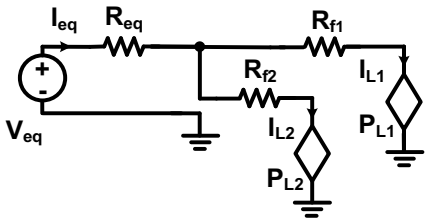

Fig. 13. The Thevenin equivalent circuit model.

Considering the characteristics of the given parameters, the parameters R_{eq} and V_{eq} of the Thevenin equivalent circuit are solved as follows:

$$R_{eq} = \frac{1}{2} \cdot \left(\frac{R_{p1}R_{q1}}{R_{p1} + R_{q1}} + R_{t1}\right) \quad (51)$$

$$V_{eq} = V_{s1} \quad (52)$$

This article has been accepted for publication in a future issue of this journal, but has not been fully edited. Content may change prior to final publication. Citation information: DOI 10.1109/TSG.2021.3081573, IEEE Transactions on Smart Grid

As per our assumption, both CPLs in the DC microgrid are working in constant power mode. Then we obtain the following power balancing equations of the model:

$$\begin{cases} P_{L1} = V_{eq} \cdot I_{L1} - {I_{L1}}^2 (R_{eq} + R_{f1}) - R_{eq} I_{L1} I_{L2} \\ P_{L2} = V_{eq} \cdot I_{L2} - {I_{L2}}^2 (R_{eq} + R_{f2}) - R_{eq} I_{L1} I_{L2} \end{cases} \quad (53)$$

Solving the power balancing equations, we get four equilibrium points of the model, as shown in the following table:

TABLE III. EQUILIBRIUM POINTS IN THE MICROGRID MODEL

Equilibrium	1st	2nd	3rd	4th
${I_{L1}}^*$	1.1338	15.4912	10.2877	3.1258
${I_{L2}}^*$	2.2829	5.3914	14.3068	19.8052

Second, we identify the stable equilibrium point(s) using Theorem 1. The analysis shows that there exists only one stable equilibrium point, that is, $({I_{L1}}^*, {I_{L2}}^*) = (1.1338, 2.2829)(\mathrm{A})$. The corresponding steady-state load voltages are $({V_{L1}}^*, {V_{L2}}^*) = (176, 175)(V)$. The identification of the stable equilibrium point is presented in Appendix D.

B. ROA Estimation

In this section, we estimate the ROA of the stable equilibrium point using the approach proposed in section IV. The stable equilibrium point is solved at the end of section V. A.

First, we formulate the optimization problem to solve the boundary c of ROA as follows:

$$c = \min_{\hat{x}} \ \hat{x}^T H_{x_e} \hat{x} \quad (54)$$

$$\text{s.t.} \begin{cases} \lambda \widehat{Q} + T_1 + T_2 \prec 0 \\ T_3 + (\lambda - 1)\widehat{Q} \succ 0 \end{cases} \quad (55)$$

Then we investigate the convexity of the feasible region of the optimization problem.

1) First, we discuss the convexity of $\lambda \widehat{Q} + T_1 + T_2 \prec 0$.

According to the derivatives in section IV, we conclude that:

(a) If ${2K_1}^i + {K_0}^i \geq 0$, the solution of $f_{\mu i}(\hat{v}_i) < 0$ is convex.

(b) If ${2K_1}^i + {K_0}^i < 0$, the solution of $f_{\mu i}(\hat{v}_i) < 0$ is not convex.

In case (b) we choose a convex subset as follows:

$$L_3(\hat{v}_i, \hat{I}_{fi}, \hat{v}_T) > \frac{1}{2{v_i}^{*2}} \left(2{K_1}^i + {K_0}^i\right)\left[\left(v_i^* + \hat{v}_{i\_min}\right)^3 + 3\left(v_i^* + \hat{v}_{i\_min}\right)^2 \left(\hat{v}_i - \hat{v}_{i\_min}\right)\right], (\hat{v}_i \geq \hat{v}_{i\_min}) \quad (56)$$

Combining case (a) with case (b), it is concluded that the convex subset of the solution of $\lambda \widehat{Q} + T_1 + T_2 \prec 0$ is the intersection set of all convex sets/subsets corresponding to each load branch respectively.

Considering that there are two CPLs in this model, the dimension of $\lambda \widehat{Q} + T_1 + T_2$ is 2. Set $\lambda = 1.3e - 4$. It is verified that ${2K_1}^i + {K_0}^i < 0, \forall i \in \{1, 2\}$. Therefore, we choose the convex subsets in the form of

$$L_3(\hat{v}_i, \hat{I}_{fi}, \hat{v}_T) > a\hat{v}_i + b, (\hat{v}_i \geq \hat{v}_{i\_min}) \quad (57)$$

where a, b are constant. Denote the subsets by $S_i, i \in \{1, 2\}$, respectively.

2) Second, we discuss the convexity of $T_3 + (\lambda - 1)\widehat{Q} \succ 0$.

As proved in section IV, we can choose a convex subset Θ of the solution of $T_3 + (\lambda - 1)\widehat{Q} \succ 0$ in the form of

$$\Theta: l_{bi} \leq \hat{v}_i \leq u_{bi}, \forall i \in \{1, 2, \dots, M\} \quad (58)$$

The set Θ can be determined with low computational cost using a binary search algorithm. In this example, set Θ is solved as:

$$\Theta: -12 \leq \hat{v}_1 \leq 7, -3 \leq \hat{v}_2 \leq 17 \quad (59)$$

3) Third, we formulate the optimization problem to estimate ROA.

$$c = \min_{\hat{x}} \ \hat{x}^T H_{x_e} \hat{x} \quad (60)$$

$$\text{s.t. } \partial\{S \cap \Theta\} \quad (61)$$

where $\partial\{S \cap \Theta\}$ represents the *boundary* of set $\{S \cap \Theta\}$. The obtained ROA is in the form of $\{\Omega_c: \hat{x}^T H_{x_e} \hat{x} \leq c\}$.

This optimization problem is solved by dividing it into multiple sub-problems. The objective function remains unchanged, and the feasible region is divided into multiple parts that are separately considered in different sub-problems.

TABLE IV. THE ORIGINAL OPTIMIZATION PROBLEM AND ITS SUB-PROBLEMS

Original optimization problem	Original feasible set $\partial\{S \cap \Theta\}$	Optimal solution c
Sub-problems	s.t. $\partial\{S_1\} \cap S_2 \cap \Theta$	$c_1 = 73820$
	s.t. $\partial\{S_2\} \cap S_1 \cap \Theta$	$c_2 = 117318$
	s.t. $\partial\{\Theta\} \cap S_1 \cap S_2$	$c_3 = 112$

It is concluded from Table IV that the optimal solution to the original optimization problem is $c = \min\{c_1, c_2, c_3\} = 112$. Therefore, the estimated ROA is $\{\Omega_c: \hat{x}^T H_{x_e} \hat{x} \leq 112\}$.

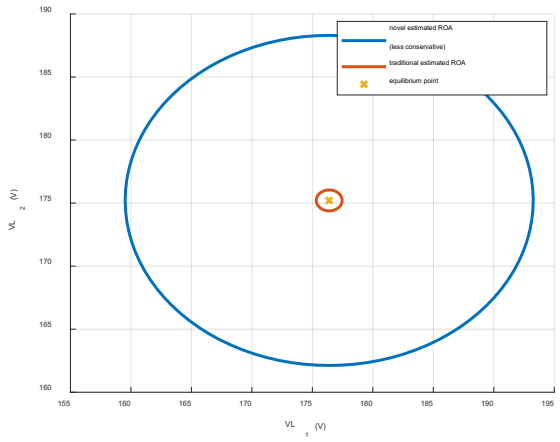

Fig. 14. The novel estimated ROA with less conservativeness vs. the traditional estimated ROA.

We visualize the ROA in the subspace consisting of the load voltages (V_{L1}, V_{L2}) in Fig. 14. The yellow cross represents the stable equilibrium point, and the blue ellipse represents the estimated ROA using our proposed method. The red ellipse represents the benchmark ROA obtained by the traditional Lyapunov method introduced in [21]. The benchmark ROA is solved as $\Omega_{c1} = \{x \in \mathcal{R}^n, \hat{x}^T H_{x_e} \hat{x} \leq 0.4490\}$. The derivatives are shown Appendix E. It is observed that the novel estimated ROA is less conservative than the benchmark ROA.

Moreover, we validate the system stability and the correctness of the estimated ROA through MATLAB/Simulink simulations. Considering that it is not practical to test all points in the estimated ROA using simulations, we test several typical data points and present the verification results here. The function values of

$L(x) = \hat{x}^T H_{x_e} \hat{x}$ at the chosen data points are very close to the solved c value, which is the estimated upper bound of $L(x)$. In this case study, we have $c = 112$. The chosen data points are represented by the "+" signs in Fig. 15. The dimension of the ROA is 13. Nevertheless, in order to formulate the cases with more typical disturbances and have a better visualization, we consider the cases with the largest oscillations of PoL voltages. In other words, we suppose the PoL voltage has the largest initial voltage difference compared to the equilibrium state $(V_{L1}{}^*, V_{L2}{}^*) = (176,175)(V)$.

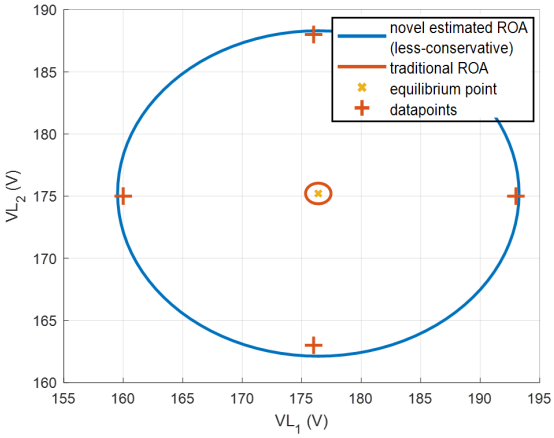

Fig. 15. Tested datapoints in the novel estimated ROA.

More details about the chosen data points are introduced in the following table.

TABLE V. DESCRIPTIONS OF THE TEST DATA POINTS

Tested data points	Position in Fig. 15	$(V_{L1}, V_{L2})(V)$	$L(x)$ value	System stability
Datapoint 1	Right	(193,175)	105.6567	Stable
Datapoint 2	Left	(160,175)	110.0692	Stable
Datapoint 3	Up	(176,188)	101.4380	Stable
Datapoint 4	Down	(176,163)	104.1449	Stable

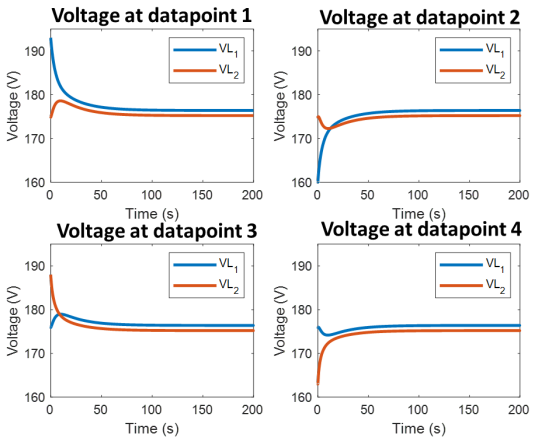

Fig. 16. Simulation results of PoL voltages.

A disturbance usually considered in large-signal stability analysis is the start-up of the system. The microgrid system is going through a significant load change during its start-up. The stability of a microgrid which has suffered the disturbance of load change can be evaluated by applying the proposed novel method to the microgrid with updated system parameters.

In this case study, we investigate the system stability with the disturbance of system start-up. The microgrid stability at these chosen data points is evaluated in the MATLAB/Simulink platform. The simulation results are shown in Fig. 16. It can be seen from Fig. 16 that the load voltages at PoLs converge to the equilibrium point as we expected in all cases. The simulation results validate the effectiveness of the proposed novel ROA estimation approach.

VII. CONCLUSIONS & FUTURE WORK

In this paper, we propose a novel approach to ROA estimation in complex DC microgrids from the perspective of potential theory. Specifically, we investigate the ROA estimation method with less conservativeness using a revised Brayton-Moser mixed potential theory. The approach targets the nonlinear microgrid model itself instead of the linearized model, which improves the algorithm accuracy. Moreover, our proposed approach is scalable in large-scale DC power grids with algorithm strategies. For example, we separate the state variables with strong relationships to stability from those with weak relationships. This strategy reduces the computational cost and lessens the curse of dimensionality. It is also verified in our case study that our approach obtains a less-conservative ROA compared to the traditional Lyapunov method. Our future work will discuss ROA estimation methods in complex power grids with stochastic environments.

VIII. ACKNOWLEDGMENT

The work was in part supported by the U.S. National Science Foundation (NSF) under Award# 2034938.

The authors also would like to thank the anonymous editors and reviewers for their valuable comments and suggestions to improve the quality of this paper.

IX. REFERENCES

[1] X. Cui, A. Avestruz, "A New Framework for Cycle-by-Cycle Digital Control of Megahertz-Range Variable Frequency Buck Converters," *2018 IEEE 19th Workshop on Control and Modeling for Power Electronics,* Padua, 2018, pp. 1-8.

[2] T. K. Roy and M. A. Mahmud, "Dynamic Stability Analysis of Hybrid Islanded DC Microgrids Using a Nonlinear Backstepping Approach," in *IEEE Systems Journal*, vol. 12, no. 4, pp. 3120-3130, Dec. 2018.

[3] A. Iovine, G. Damm, E. D. Santis, M. D. Di Benedetto, L. Galai-Dol and P. Pepe, "Voltage Stabilization in a DC MicroGrid by an ISS-like Lyapunov Function implementing Droop Control," *2018 European Control Conference (ECC)*, Limassol, 2018, pp. 1130-1135.

[4] F. Perez, A. Iovine, G. Damm, L. Galai-Dol and P. F. Ribeiro, "Stability Analysis of a DC MicroGrid for a Smart Railway Station Integrating Renewable Sources," in *IEEE Transactions on Control Systems Technology*, vol. 28, no. 5, pp. 1802-1816, Sept. 2020.

[5] M. A. Hassan, E. Li, X. Li, T. Li, C. Duan and S. Chi, "Adaptive Passivity-Based Control of dc–dc Buck Power Converter With Constant Power Load in DC Microgrid Systems," in *IEEE Journal of Emerging and Selected Topics in Power Electronics*, vol. 7, no. 3, pp. 2029-2040, Sept. 2019.

[6] D. Marx, S. Pierfederici, B. Nahid-Mobarakeh and B. Davat, "Contribution to Determination of Domain of Attraction in Power Systems: Application to Drives with Input Filter," 2009 IEEE Industry Applications Society Annual Meeting, Houston, TX, 2009, pp. 1-8.

[7] B. Loop, S. Sudhoff, S. Żak, E. L. Zivi, "Estimating Regions of Asymptotic Stability of Power Electronics Systems Using Genetic Algorithms," in *IEEE Trans on Control Systems Technology*, vol.18, no.5, pp.1011-1022, Sept. 2010.

[8] D. Marx, P. Magne, B. Nahid-Mobarakeh, S. Pierfederici and B. Davat, "Large Signal Stability Analysis Tools in DC Power Systems With Constant Power Loads and Variable Power Loads—A Review," in IEEE Transactions on Power Electronics, vol. 27, no. 4, pp. 1773-1787, April 2012.

[9] A. Bacha, H. Jerbi and N. B. Braiek, "An Approach of Asymptotic Stability Domain Estimation of Discrete Polynomial Systems," *The Proceedings of the Multiconference on "Computational Engineering in Systems Applications*, Beijing, 2006, pp. 288-292.
[10] T. L. Vu and K. Turitsyn, "Lyapunov Functions Family Approach to Transient Stability Assessment," in *IEEE Transactions on Power Systems*, vol. 31, no. 2, pp. 1269-1277, March 2016.
[11] F. Chang, X. Cui, M. Wang, W. Su and A. Q. Huang, "Large-Signal Stability Criteria in DC Power Grids With Distributed-Controlled Converters and Constant Power Loads," in *IEEE Transactions on Smart Grid*, vol. 11, no. 6, pp. 5273-5287, Nov. 2020.
[12] R. K. Brayton and J. K. Moser, "A theory of nonlinear networks. I," in *Quarterly of Applied Mathematics*, vol. 22, no.1, pp. 1–33, 1964.
[13] A. Papachristodoulou and S. Prajna, "A tutorial on sum of squares techniques for systems analysis," Proceedings of the 2005, *American Control Conference*, 2005., Portland, OR, USA, 2005, pp. 2686-2700 vol. 4.
[14] Izumi, S., Somekawa, H., Xin, X. *et al.* "Estimation of regions of attraction of power systems by using sum of squares programming," *Electr Eng* **100,** 2205–2216 (2018).
[15] Chesi, Graziano. *Domain of attraction: analysis and control via SOS programming*. Vol. 415. Springer Science & Business Media, 2011.
[16] S. K. Mazumder and E. Pilo de la Fuente, "Stability Analysis of Micropower Network," in *IEEE Journal of Emerging and Selected Topics in Power Electronics*, vol. 4, no. 4, pp. 1299-1309, Dec. 2016.
[17] Y. Chen, M. Tanaka, K. Tanaka and H. O. Wang, "Stability Analysis and Region-of-Attraction Estimation Using Piecewise Polynomial Lyapunov Functions: Polynomial Fuzzy Model Approach," in *IEEE Transactions on Fuzzy Systems*, vol. 23, no. 4, pp. 1314-1322, Aug. 2015.
[18] M. Vatani and M. Hovd, "Lyapunov stability analysis and controller design for rational polynomial systems using sum of squares programming," *IEEE Annual Conference on Decision and Control*, Melbourne, VIC, 2017, pp. 4266-4271.
[19] J. LaSalle, "Some extensions of Liapunov's second method," *IRE Transactions on Circuit Theory*, CT-7, pp. 520–527, 1960.
[20] H. K. Khalil, *Nonlinear Systems*. Upper Saddle River (2002), pp. 136–139.
[21] H. K. Khalil, *Nonlinear Systems*. Upper Saddle River (2002), pp. 316–320.

Appendix A

Proof: The proof of the stability of the equilibrium point $x = x_e$ is proposed in our previous study [11]. Here we show the proof of the existence of a Lyapunov function.

As introduced in the previous section, the grid model with dynamics can be described as

$$\nabla P^* = -J^* \dot{x} \tag{62}$$

where $x = [i \;\; v]^T$, $J^* \succ 0$ for stable systems. J^* does not need to be a symmetric matrix, considering that $J^* \succ 0$, $(J^*)^{-1}$ exists. Then the above system can be equivalently formulated as follows:

$$\dot{x} = -(J^*)^{-1} \nabla P^* \tag{63}$$

Linearizing the system at equilibrium $x = x_e$, we have:

$$\begin{aligned} \dot{\hat{x}} &= \mathcal{J}(-(J^*)^{-1}\nabla P^*)|_{x=x_e} \cdot \hat{x} \\ &= -(J^*)^{-1}(\mathcal{J}(\nabla P^*))|_{x=x_e} \cdot \hat{x} \\ &= -(J^*)^{-1} H(P^*)|_{x=x_e} \cdot \hat{x} \end{aligned} \tag{64}$$

where $\hat{x} = x - x_e$. $\mathcal{J}$ is the Jacobian matrix and H is the Hessian matrix. Define $A = -(J^*)^{-1} H(P^*)|_{x=x_e}$. Then we obtain the linearized system:

$$\dot{\hat{x}} = A\hat{x} \tag{65}$$

Adding the residual term, we get the original nonlinear system as follows:

$$\dot{x} = A\hat{x} + g(\hat{x}) \tag{66}$$

where $g(\hat{x}) = f(\hat{x} + x_e) - A\hat{x}$.

A Lyapunov function can be constructed as follows:

$$L = (x - x_e)^T N (x - x_e), \tag{67}$$

where N is the positive definite solution of the following Lyapunov equation:

$$A^T N + NA = -Q, Q \succ 0 \tag{68}$$

From $J^* \succ 0$, we conclude that $(J^*)^T \succ 0$ and $(J^*)^{-1} \succ 0$;

Considering that $H(P^*)|_{x=x_e} \succ 0$, $J^* \succ 0$, the eigenvalues of $(J^*)^{-1} \cdot H(P^*)|_{x=x_e}$ have positive real parts. Therefore, all eigenvalues of $A = -(J^*)^{-1} H(P^*)|_{x=x_e}$ have a negative real part, that is, matrix A is Hurwitz. Therefore, N exists and is the unique solution of the Lyapunov equation [20].

Appendix B

Suppose

$$Q = -\begin{bmatrix} Q_{11} & Q_{12} \\ Q_{21} & \hat{Q} \end{bmatrix}, H_{x_e} = \begin{bmatrix} H_{11} & H_{12} \\ H_{21} & \hat{H} \end{bmatrix} \tag{69}$$

where $Q_{11} \in \mathcal{R}^{(4N+M+1)\times(4N+M+1)}$,
$H_{11} \in \mathcal{R}^{(4N+M+1)\times(4N+M+1)}, \hat{Q} \in \mathcal{R}^{M\times M}, \hat{H} \in \mathcal{R}^{M\times M}$.

Denote $\hat{x} = [\hat{x}_a{}^T, \hat{V}_L{}^T]^T$, where $V_L = [V_{L1}, \dots, V_{LM}]$, $x_a = [I_{p1}, \dots, I_{pN}, I_{q1}, \dots, I_{qN}, I_{t1}, \dots, I_{tN}, I_{f1}, \dots, I_{fM}, V_{C1}, \dots, V_{CN}, V_D]$.

Then the Hessian of $\dot{V}(\hat{x})$ can be calculated as follows.

$$\begin{aligned} 2\hat{x}^T H_{x_e} g(x) &= 2\left[\hat{x}_a{}^T, \hat{V}_L{}^T\right]^T \begin{bmatrix} H_{11} & H_{12} \\ H_{21} & \hat{H} \end{bmatrix} \left[0, \Phi(\hat{V}_L)\right]^T \\ &= 2(\hat{x}_a{}^T H_{12} + \hat{V}_L{}^T \hat{H})\Phi(\hat{V}_L) \end{aligned} \tag{70}$$

The gradient and the Hessian of $2\hat{x}^T H_{x_e} g(x)$ are calculated as follows:

$$\begin{aligned} &\nabla\left(2\hat{x}^T H_{x_e} g(\hat{x})\right) \\ &= 2\left[H_{12}\Phi(\hat{V}_L), \hat{x}_a H_{12} \nabla_c \Phi(\hat{V}_L) + \nabla(\hat{V}_L{}^T \hat{H} \Phi(\hat{V}_L))\right]^T \end{aligned} \tag{71}$$

$$\begin{aligned} &\nabla^2\left(2\hat{x}^T H_{x_e} g(\hat{x})\right) \\ &= 2\begin{bmatrix} \mathbf{0} & H_{12}\nabla_c\Phi(\hat{V}_L) \\ (H_{12}\nabla_c\Phi(\hat{V}_L))^T & \nabla^2\left(\hat{V}_L{}^T \hat{H}\Phi(\hat{V}_L)\right) + \hat{x}_a H_{12} \nabla_c{}^2 \Phi(\hat{V}_L) \end{bmatrix} \end{aligned} \tag{72}$$

Considering that

$$\dot{V}(\hat{x}) = \hat{x}^T\left[\nabla f^T(x_e) H_{x_e} + H_{x_e} \nabla f(x_e)\right]\hat{x} + 2\hat{x}^T H_{x_e} g(\hat{x}) \tag{73}$$

$$Q = -(\nabla f^T(x_e) H_{x_e} + H_{x_e} \nabla f(x_e)) \tag{74}$$

then the Hessian of $\dot{V}(\hat{x})$ is calculated as follows:

$$\begin{aligned} &\nabla^2 \dot{V}(\hat{x}) \\ &= Q + 2\begin{bmatrix} \mathbf{0} & H_{12}\nabla_c\Phi(\hat{V}_L) \\ \left(H_{12}\nabla_c\Phi(\hat{V}_L)\right)^T & \nabla^2\left(\hat{V}_L{}^T \hat{H}\Phi(\hat{V}_L)\right) + \hat{x}_a H_{12}\nabla_c{}^2\Phi(\hat{V}_L) \end{bmatrix} \\ &= \begin{bmatrix} Q_{11} & Q_{12} + 2H_{12}\nabla_c\Phi(\hat{V}_L) \\ Q_{21} + 2(H_{12}\nabla_c\Phi(\hat{V}_L))^T & \hat{Q} + 2\nabla^2\left(\hat{V}_L{}^T \hat{H}\Phi(\hat{V}_L)\right) + 2\hat{x}_a H_{12}\nabla_c{}^2\Phi(\hat{V}_L) \end{bmatrix} \end{aligned} \tag{75}$$

where $\nabla_c\Phi(\hat{V}_L) = diag\{\nabla\varphi_1(\hat{v}_1), \dots, \nabla\varphi_M(\hat{v}_M)\}, \nabla_c{}^2\Phi(\hat{V}_L) = diag\{\nabla^2\varphi_1(\hat{v}_1), \dots, \nabla^2\varphi_M(\hat{v}_M)\}$.

Appendix C

$$\begin{aligned} &f_{\mu i}(\hat{v}_i) \\ &= \lambda\hat{Q}_i + 2\frac{d^2}{d\hat{v}_i{}^2}\left(-\frac{P_{Li}}{v_i{}^{*2}} + 2R_{fi}\right)\hat{v}_i\varphi_i(\hat{v}_i) + 2\frac{d^2}{d\hat{v}_i{}^2}\varphi_i(\hat{v}_i)\left(\hat{I}_{fi} - \hat{v}_T R_{fi}\right) \\ &= K_0{}^i + \sigma''\left(K_1{}^i\hat{v}_i + 2K_2{}^i L_1(\hat{I}_{fi}, \hat{v}_T)\right) + 2K_1{}^i\sigma' \end{aligned} \tag{76}$$

This article has been accepted for publication in a future issue of this journal, but has not been fully edited. Content may change prior to final publication. Citation information: DOI 10.1109/TSG.2021.3081573, IEEE Transactions on Smart Grid

where $K_0{}^i = \lambda\hat{Q}_i, K_1{}^i = 2\left(-\frac{P_{Li}}{v_i{}^{*2}} + 2R_{fi}\right)\left(-\frac{P_{Li}}{C_{Li}}\frac{1}{v_i{}^{*2}}\right), K_2{}^i = -\frac{P_{Li}}{C_{Li}}\frac{1}{v_i{}^{*2}}, L_1\left(\hat{I}_{fi}, \hat{v}_T\right) = \hat{I}_{fi} - \hat{v}_T R_{fi}, \sigma(\hat{v}_i) = \frac{\hat{v}_i{}^2}{v_i{}^* + \hat{v}_i}, i = 1,2,\dots,M.$

Denote $L_2\left(\hat{v}_i, \hat{I}_{fi}, \hat{v}_T\right) = K_1{}^i\hat{v}_i + 2K_2{}^i L_1\left(\hat{I}_{fi}, \hat{v}_T\right)$.

Since $\sigma' = 1 - \frac{v_i{}^{*2}}{(v_i{}^* + \hat{v}_i)^2}, \sigma'' = \frac{2v_i{}^{*2}}{(v_i{}^* + \hat{v}_i)^3} > 0$, we have

$$\begin{aligned} & f_{\mu i}(\hat{v}_i) < 0 \\ \Leftrightarrow\ & L_2\left(\hat{v}_i, \hat{I}_{fi}, \hat{v}_T\right) < \frac{-2K_1{}^i\sigma' - K_0{}^i}{\sigma''} \\ =\ & -\frac{2K_1{}^i + K_0{}^i}{2v_i{}^{*2}}(v_i{}^* + \hat{v}_i)^3 + K_1{}^i(v_i{}^* + \hat{v}_i) \end{aligned} \quad (77)$$

Define $L_3\left(\hat{v}_i, \hat{I}_{fi}, \hat{v}_T\right) \triangleq K_1{}^i(v_i{}^* + \hat{v}_i) - L_2\left(\hat{v}_i, \hat{I}_{fi}, \hat{v}_T\right)$. Then we have

$$f_{\mu i}(\hat{v}_i) < 0 \Leftrightarrow L_3\left(\hat{v}_i, \hat{I}_{fi}, \hat{v}_T\right) > \frac{2K_1{}^i + K_0{}^i}{2v_i{}^{*2}}(v_i{}^* + \hat{v}_i)^3 \quad (78)$$

Additionally, it is worth mentioning that $L_3\left(\hat{v}_i, \hat{I}_{fi}, \hat{v}_T\right)$ is a linear function.

$$\begin{aligned} L_3\left(\hat{v}_i, \hat{I}_{fi}, \hat{v}_T\right) &= K_1{}^i(v_i{}^* + \hat{v}_i) - K_1{}^i\hat{v}_i - 2K_2{}^i L_1\left(\hat{I}_{fi}, \hat{v}_T\right) \\ &= -2K_2{}^i L_1\left(\hat{I}_{fi}, \hat{v}_T\right) + K_1{}^i v_i{}^* \end{aligned} \quad (79)$$

When $2K_1{}^i + K_0{}^i \geq 0$, it can be proved that the solution of $f_{\mu i}(\hat{v}_i) < 0$ is convex as follows.

Suppose

$$g\left(\hat{v}_i, \hat{I}_{fi}, \hat{v}_T\right) \triangleq \frac{1}{2v_i{}^{*2}}(2K_1{}^i + K_0{}^i)(v_i{}^* + \hat{v}_i)^3 \quad (80)$$

Then

$$f_{\mu i}(\hat{v}_i) < 0 \Leftrightarrow L_3\left(\hat{v}_i, \hat{I}_{fi}, \hat{v}_T\right) > g\left(\hat{v}_i, \hat{I}_{fi}, \hat{v}_T\right) \quad (81)$$

Denote $\hat{x} = [\hat{v}_i, \hat{I}_{fi}, \hat{v}_T]$.

Considering that $v_i = v_i{}^* + \hat{v}_i > 0, g\left(\hat{v}_i, \hat{I}_{fi}, \hat{v}_T\right)$ is a convex function, then $\forall x_1, x_2, \alpha \in [0,1]$,

$$s.t. \quad \begin{cases} L_3(\widehat{x_1}) > g(\widehat{x_1}) \\ L_3(\widehat{x_2}) > g(\widehat{x_2}) \end{cases}, \quad (82)$$

and the following formulation holds:

$$\begin{aligned} L_3(\alpha\widehat{x_1} + (1-\alpha)\widehat{x_2}) &= \alpha L_3(\widehat{x_1}) + (1-\alpha)L_3(\widehat{x_2}) \\ &> \alpha g(x_1) + (1-\alpha)g(x_2) \\ &> g(\alpha\widehat{x_1} + (1-\alpha)\widehat{x_2}) \end{aligned} \quad (83)$$

Therefore, the solution of $L_3\left(\hat{v}_i, \hat{I}_{fi}, \hat{v}_T\right) > g\left(\hat{v}_i, \hat{I}_{fi}, \hat{v}_T\right)$ is a convex set. In other words, the solution of $f_{\mu i}(\hat{v}_i) < 0$ is convex.

Appendix D

The potential function of the model is calculated as follows.

$$\begin{aligned} P(i,v) = & \sum_{i=1}^{2} V_{refi}\left(I_{pi} + I_{qi}\right) - \frac{1}{2}\sum_{i=1}^{2} R_{pi}I_{pi}{}^2 - \frac{1}{2}\sum_{i=1}^{2} R_{qi}I_{qi}{}^2 \\ & - \frac{1}{2}\sum_{i=1}^{2} R_{ti}I_{ti}{}^2 - \frac{1}{2}\sum_{i=1}^{2} R_{fi}I_{fi}{}^2 - \sum_{i=1}^{2} V_{Ci}\left(I_{pi} + I_{qi} - I_{ti}\right) \\ & - V_D\left(\sum_{i=1}^{2} I_{ti} - \sum_{i=1}^{2} I_{fi}\right) + \sum_{i=1}^{2} Z_i(i,v) \end{aligned} \quad (84)$$

where

$$Z_i(i,v) = \begin{cases} \int_{V_{min}}^{V_{Li}} \frac{P_{Li}}{v}dv - P_{Li} - V_{Li}(I_{fi} - I_{Li}), V_{Li} > V_{\min\_i} \\ I_{\max\_i}(V_{Li} - V_{\min\_i}) - P_{Li} - V_{Li}(I_{fi} - I_{\max\_i}), V_{Li} \leq V_{\min\_i} \end{cases} \quad (85)$$

I_{pi} and I_{qi} represent the currents through resistors R_{pi} and R_{qi}, respectively.

Add virtual inductors $L_{pi} = 0$ in series with R_{pi} for $i = \{1,2\}$ in the original model. Then we define the following notations:

$$\begin{aligned} & R = diag\left(\left[R_{p1}, R_{p2}, R_{q1}, R_{q2}, R_{t1}, R_{t2}, R_{f1}, R_{f2}\right]\right) \\ & = diag\left(\left[R_p, R_q, R_t, R_f\right]\right), \\ & L = diag\left(\left[L_{p1}, L_{p2}, L_{q1}, L_{q2}, L_{t1}, L_{t2}, L_{f1}, L_{f2}\right]\right) \\ & = diag\left(\left[L_p, L_q, L_t, L_f\right]\right), \\ & C = diag\left(\left[C_{b1}, C_{b2}, C_D, C_{f1}, C_{f2}\right]\right) = diag\left(\left[C_b, C_D, C_f\right]\right), \\ & i = \left[I_{p1}, I_{p2}, I_{q1}, I_{q2}, I_{t1}, I_{t2}, I_{f1}, I_{f2}\right]^T = \left[I_p, I_q, I_t, I_f\right]^T, \\ & v = [V_{C1}, V_{C2}, V_D, V_{L1}, V_{L2}]^T = [V_C, V_D, V_L]^T. \end{aligned}$$

Then the above potential function can be rewritten in the form of

$$P(i,v) = -\frac{1}{2}(i, Ai) + B(v) + (i, \gamma v - a) \quad (86)$$

where $A: \mathbb{R}^6 \to \mathbb{R}, B: \mathbb{R}^3 \to \mathbb{R}, \gamma$ is a constant matrix and a is a constant vector; $(\cdot, \cdot)$ represents an inner product. It is obtained that

$$A = \frac{1}{2}i^T Ri, \qquad \gamma = \begin{bmatrix} -\mathbb{I}_{2\times2} & 0_{2\times1} & 0_{2\times2} \\ -\mathbb{I}_{2\times2} & 0_{2\times1} & 0_{2\times2} \\ \mathbb{I}_{2\times2} & -1_{2\times1} & 0_{2\times2} \\ 0_{2\times2} & 1_{2\times1} & -\mathbb{I}_{2\times2} \end{bmatrix}_{8\times5}, \quad (87)$$

$$B(v) = \sum_{i=1}^{2} b_i(v), \quad (88)$$

$$b_i(v) = \begin{cases} P_{Li}\ (\ln V_{Li} - \ln V_{\min\_i}), V_{Li} > V_{\min\_i} \\ I_{\max\_i}\ V_{Li} - I_{\max\_i}\ V_{\min\_i}, V_{Li} \leq V_{\min\_i} \end{cases} \quad (89)$$

where $\mathbb{I}$ is an identity matrix.

Next, we rigorously examine the stability of the equilibrium points using the proposed sufficient condition for stability in our previous study [11].

1) First, it is verified that $f(x) = \dot{x}: \mathcal{R}^n \to \mathcal{R}$ is a C^1 function and $P^*: \mathcal{R}^n \to \mathcal{R}$ is a C^2 function. Additionally, all equilibrium points of the system form a compact set because the number of equilibrium points in this model is finite.

2) $J^* \succ 0$. This condition is equivalent to

$$\sigma_{max}\left(L^{1/2}A^{-1}\gamma C^{-1/2}\right) < 1 \quad (90)$$

where $\sigma_{max}(\cdot)$ represents the largest singular value.

3) $H(P^*)|_{x=x_e} \succeq 0$. This condition is equivalent to the following equation:

$$\frac{\partial^2 B(v)}{\partial v^2} + \gamma^T A^{-1}\gamma\Big|_{v=v_e} \succeq 0 \quad (91)$$

Considering that

This article has been accepted for publication in a future issue of this journal, but has not been fully edited. Content may change prior to final publication. Citation information: DOI 10.1109/TSG.2021.3081573, IEEE Transactions on Smart Grid

$$\frac{\partial^2 b_i(v)}{\partial v^2} = \begin{cases} -\frac{P_{Li}}{{V_{Li}}^2}, & V_{Li} > V_{\min\_i} \\ 0, & V_{Li} \le V_{\min\_i} \end{cases} \quad (92)$$

we have

$$\frac{\partial^2 B(v)}{\partial v^2} = diag\{0,0,0,\frac{\partial^2 b_1(v)}{\partial v^2},\frac{\partial^2 b_2(v)}{\partial v^2}\} \quad (93)$$

4) $P^*(x)$ is radially unbounded, i.e., $P^*(x) \to \infty$ as $\|x\| \to \infty$. This condition is checked directly in specific circuits.

We obtain the stable equilibrium points of the model after testing all existing equilibrium points using the above four conditions.

Appendix E

Pick up $N = H(P^*)|_{x=x_e} \succ 0$. Then the Lyapunov function $L(x)$ is constructed as

$$L = \hat{x}^T N \hat{x}, \quad (94)$$

where $\hat{x} = x - x_e$. The derivative of the Lyapunov function dL/dt is solved as follows:

$$\begin{aligned} \frac{dL}{dt} &= \dot{\hat{x}}^T N\hat{x} + \hat{x}^T N\dot{\hat{x}} \\ &= \big(\hat{x}^T A^T + g^T(\hat{x})\big)N\hat{x} + \hat{x}^T N\big(A\hat{x} + g(\hat{x})\big) \\ &= \hat{x}^T(A^T N + NA)\hat{x} + 2\hat{x}^T N g(\hat{x}) \\ &= -\hat{x}^T Q\hat{x} + 2\hat{x}^T N g(\hat{x}) \end{aligned} \quad (95)$$

where $g(\hat{x}) = f(\hat{x} + x_e) - A\hat{x}$, $Q = A^T N + NA \succ 0$.

Because $\|g(\hat{x})\|_2 = o(\|\hat{x}\|_2)$, there exists $\gamma > 0$ such that

$$\forall \|\hat{x}\| \le \gamma, \qquad \|g(\hat{x})\|_2 < \alpha\|\hat{x}\|_2 \quad (96)$$

where $\alpha \in \mathcal{R}^+$. Then we have

$$\begin{aligned} \frac{dL}{dt} &= -\hat{x}^T Q\hat{x} + 2(N^T\hat{x})^T g(\hat{x}) \\ &\le -\lambda_{min}(Q)\|\hat{x}\|^2 + 2\|N^T\hat{x}\|\|g(\hat{x})\| \\ &\le -\lambda_{min}(Q)\|\hat{x}\|^2 + 2\alpha\|N^T\hat{x}\|\|\hat{x}\| \\ &\le -\lambda_{min}(Q)\|\hat{x}\|^2 + 2\alpha\lambda_{max}(N)\|\hat{x}\|^2 \end{aligned} \quad (97)$$

To guarantee $\frac{dL}{dt} \le 0$, set

$$-\lambda_{min}(Q)\|\hat{x}\|^2 + 2\alpha\lambda_{max}(N)\|\hat{x}\|^2 \le 0 \quad (98)$$

Then α is solved as

$$\alpha \le \frac{\lambda_{min}(Q)}{2\lambda_{max}(N)} \quad (99)$$

Next, we solve γ. We have

$$\forall \|\hat{x}\| \le \gamma, \qquad \|g(\hat{x})\|_2 < \alpha\|\hat{x}\|_2 \quad (100)$$

We know

$$\begin{aligned} g(\hat{x}) &= f(\hat{x} + x_e) - A\hat{x} \\ &= \dot{x} + (J^*)^{-1}H(P^*)|_{x=x_e}\hat{x} \\ &= \dot{x} - \nabla f(x)|_{x=x_e}\hat{x} \end{aligned} \quad (101)$$

Denote the elements in the vector $g(\hat{x})$ by $g_k(\widehat{x_k}), k = 1,2,\dots,N+M$. The fact is that $g_k(\widehat{x_k}) = 0$ for variable x_k: $\dot{x}_k = f_k(x_k)$ if $f_k(x_k)$ is linear. In the proposed microgrid model, the state variables $I_{pi}, I_{qi}, I_{ti}, I_{fj}, V_{Ci}$ $(i = 1,2,\dots,N, j = 1,2,\dots,M)$ are under this situation. Moreover, $g_k(\widehat{x_k}) \neq 0$ for variables V_{Lj} $(j = 1,2,\dots,M)$ because these state variables involve nonlinear dynamic functions. Considering that

$$\dot{V_{Lj}} = f_k(x) = \frac{1}{C_{fj}}(i_{fj} - \frac{P_{Lj}}{V_{Lj}}) \quad (102)$$

Then we can calculate $g_k(\widehat{V_{Lj}})$ as follows:

$$\begin{aligned} g_k(\widehat{V_{Lj}}) &= \dot{V_{Lj}} - \nabla f_k(x)|_{V_{Lj}={V_{Lj}}^*} \cdot \hat{x} \\ &= -\frac{P_{Lj}\widehat{V_{Lj}}^2}{({V_{Lj}}^* + \widehat{V_{Lj}})C_{fj}({V_{Lj}}^*)^2} \end{aligned} \quad (103)$$

where ${V_{Lj}}^*$ is the steady-state voltage of V_{Lj}.

Next, we solve

$$\|g(\hat{x})\|_2 < \alpha\|\hat{x}\|_2 \quad (104)$$

A sufficient condition of the above inequality is as follows:

$$\|g_k(\widehat{V_{Lj}})\|_2 < \alpha\|\widehat{V_{Lj}}\|_2, \qquad \forall j = 1,2,\dots,M \quad (105)$$

Solving this expression, we obtain that

$$\widehat{V_{Lj}} = \frac{{V_{Lj}}^*(-Y_j \pm \sqrt{Y_j})}{Y_j - 1}, \forall j = 1 \dots M \quad (106)$$

where

$$Y_j = \alpha^2(\frac{C_{fj}}{P_{Lj}})^2({V_{Lj}}^*)^4 \quad (107)$$

It is worth mentioning that we need to ensure that $Y_j < 1$, which can be realized by tuning α. Then γ is solved from its definition:

$$\gamma = \min_{j\in\{1,2,\dots,M\}} \frac{{V_{Lj}}^*(Y_j - \sqrt{Y_j})}{Y_j - 1} \quad (108)$$

Then the ROA is estimated as the set $\Omega_c = \{x \in \mathcal{R}^n, L(x) \le c\}$, where

$$c \triangleq \min_{\|\hat{x}\|_2=\gamma} x^T N x = \lambda_{min}(N)\gamma^2 \quad (109)$$

$N = H(P^*)|_{x=x_e}$. The optimization problem can be solved by a quadratic programming (QP) solver.

Fangyuan Chang (S'18) received the B.S. degree in electrical engineering from North China Electric Power University, China, in 2016, and the M.S. degree in electrical engineering from the University of Michigan, Ann Arbor, MI, in 2018. She is currently working toward the Ph.D. degree at the University of Michigan, Dearborn, MI. Her research interests include power systems, control theory and machine learning.

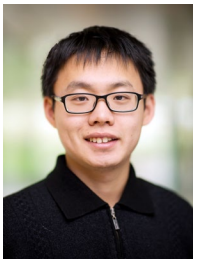

Xiaofan Cui (S'17) is currently a Ph.D. candidate in electrical engineering and computer science at the University of Michigan, Ann Arbor. He received the B.S. degree in electrical engineering and automation from Tsinghua University in 2016. He was a visiting student at Standard University during the summer of 2015. His research interests include circuit modeling, digital control, and high-performance power electronics.

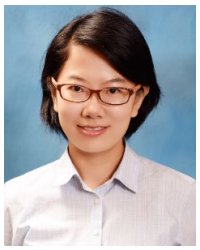

Mengqi Wang (S'11-M'15-SM'20) received the B.S. degree in electrical engineering from Xi'an Jiaotong University, Xi'an, in 2009 and the Ph.D. degree in electrical engineering from North Carolina State University, Raleigh, NC, in 2014. Since 2015, she has been an Assistant Professor in the Department of Electrical and Computer Engineering at the University of Michigan-Dearborn, USA. She is a Senior Member of IEEE. Her current research interests include DC-DC and DC-AC power conversions, high-efficiency and high power-density power supplies, renewable energy systems, and wide-bandgap power device applications.

Wengcong Su (S'06-M'13-SM'18) received the B.S. degree (with distinction) from Clarkson University, Potsdam, NY, USA, in 2008, the M.S. degree from Virginia Tech, Blacksburg, VA, USA, in 2009, and the Ph.D. degree from North Carolina State University, Raleigh, NC, USA, in 2013, respectively. He is currently an Associate Professor in the Department of Electrical and Computer Engineering at the University of Michigan-Dearborn, USA. He is a Fellow of IET and a Senior Member of IEEE. He is a registered Professional Engineer (P.E.) in the State of Michigan, USA. His current research interests include power systems, electrified transportation systems, and cyber-physical systems. He is an Editor of IEEE Transactions on Smart Grid, an Associate Editor of IEEE Access, and an Associate Editor of IEEE DataPort. He has authored one book, four book chapters, and over 100 high-quality articles in prestigious international journals and peer-reviewed conference proceedings. He was the recipient of the 2015 IEEE Power and Energy Society (PES) Technical Committee Prize Paper Award and the 2013 IEEE Industrial Electronics Society (IES) Student Best Paper Award.